The First Billion Years

REPORT OF A STUDY PROGRAM

Study start date: 16 August 2010
Study end date: 14 October 2011
Final report submission date: 1 April 2012

TEAM LEADS

Judd Bowman, ASU
Judd.Bowman@asu.edu

Steve Furlanetto, UCLA
sfurlane@ucla.edu

Dayton Jones, JPL
Dayton.Jones@jpl.nasa.gov

Anthony Readhead, Caltech
acr@astro.caltech.edu

KECK INSTITUTE FOR SPACE STUDIES
CALIFORNIA INSTITUTE OF TECHNOLOGY
JET PROPULSION LABORATORY

Study Participants

Participant	Affiliation
Yacine Ali-Haïmoud	Caltech
Jamie Bock	JPL
Geoffrey Bower	UC Berkeley
Judd Bowman	ASU
Matt Bradford	Caltech
Chris Carilli	NRAO
Tsu-Ching Chang	CITA
Ranga-Ram Chary	Caltech/IPAC
Jens Chluba	CITA, Toronto
Sarah Church	Stanford Univ.
Garret Cotter	Oxford Univ.
Asantha Cooray	UC Irvine
Dave DeBoer	UC Berkeley
Angelica de Oliveira-Costa	CfA
Roger Dean	Oxford Univ.
Olivier Doré	JPL
Steve Furlanetto	UCLA
Todd Gaier	JPL

Participant	Affiliation
Keith Grainge	Cambridge Univ.
Josh Gunderson	Univ. Miami
Chris Hirata	Caltech
Dayton Jones	JPL
Michael Jones	Oxford Univ.
Garrett Karto Keating	UC Berkeley
Charles Lawrence	JPL
Louis Levenson	Caltech
Joseph Lazio	JPL
Philip Lubin	UC Santa Barbara
Tim Pearson	Caltech
Jonathan Pritchard	Imperial College London
Anthony Pullen	Caltech
Steve Rawlings	Oxford Univ.
Tony Readhead	Caltech
Dominik Riechers	Caltech
Lorene Samoska	JPL
Mike Seiffert	JPL
Angela Taylor	Oxford Univ.

Contents

1

Executive Summary

Spectral measurements of atomic and molecular lines embedded in the cosmic microwave background (CMB) have the potential to open entirely new probes of the early Universe. Two avenues are of great interest:

1) Spectral line deviations from the CMB blackbody spectrum will enable the study of hydrogen and helium recombination physics during and before the time of the surface of last scattering, and could provide the potential for game-changing discoveries by testing dark matter annihilation in the redshift range $6000 > z > 1000$, by allowing a test of the time-dependence of the fine-structure constant at a critical epoch, and by testing inflation models using an independent method.

2) Extension of CMB anisotropy measurements to detect unresolved spectral line emission from star-forming galaxies during reionization ($6 < z < 10$) would directly delineate the large-scale structure of the galaxies responsible for reionizing the Universe and provide the only foreseeable measurements on scales sufficiently large to compare with upcoming observations of reionization by way of the redshifted hydrogen 21 cm line. CO, [C II], and Ly-α lines were investigated as promising targets. CO and [C II] line transitions emerged as particularly compelling.

The two science objectives identified in the Program share some common core technological requirements based on the shared need for approximately 1000-element feed arrays followed by broadband, high-resolution spectral correlators. The technical requirements lead to a roadmap for development of large feed arrays beginning with applications in a ground-based CO mapping instrument and leading to a space-borne recombination-line all-sky spectrometer. The key technical issues include compact and light-weight integrated spectral dual-polarization inexpensive receiver modules, large high-resolution spectral correlators (analog and/or digital), and light-weight feeds. In parallel we recommend long-term investigations into high precision calibrators and calibration techniques that will be required for the recombination line instrument. A second roadmap addresses technical developments required for a 2-D spectroscopic instrument for [C II] mapping.

2

Introduction

Of the nearly 14 billion year history of the Universe, we have only limited information about the first billion years. In this largely unexplored era of cosmic time, the Universe's "dark ages," some of the most critical events in the history of the Universe occurred, including the processes leading to the formation of the first star, the first galaxy, and the first black hole. This is the fundamental period when primordial density fluctuations following inflation evolved through baryon in-fall, adiabatic cooling, and gravitational collapse to create compact luminous structures for the first time. But probing this era is beyond the capabilities of today's instruments. New approaches are needed to enable breakthrough observations.

After decades of advances, CMB experiments are reaching the nano-kelvin sensitivity regime needed to enable atomic and molecular line observations from the redshift range $10 < z < 2000$. Such measurements would be an entirely new direction for the CMB community, which has focused to date on extracting information from the angular structure of the signal, rather than the spectral structure. At the same time, in recent years, significant effort has been invested in developing techniques to detect the combined spectral-angular signatures of intervening neutral atomic hydrogen gas during the epoch of reionization ($z \sim 10$) against the CMB backlight using the 21 cm hyperfine line of hydrogen. These techniques are about to be tested by the first generation of ground based experiments.

In addition to the developments in CMB and 21 cm techniques, significant theoretical effort has been invested recently in calculating recombination lines and later metal lines in the early Universe (e.g., Chluba and Sunyaev 2006, 2008b,c, 2009, 2010; Chluba 2010). Furthermore, ALMA, JWST and the next generation of large ground-based optical/IR telescopes will detect and characterize large numbers of high redshift ($z < 15$) objects within this decade, providing a rich catalog of sources for use with other observations, but also pushing traditional astronomical observations toward their foreseeable limits.

This Study Program focused on the convergence of these developments by convening leading observers, experimentalists, and theorists for the first time to specifically focus on the challenges and opportunities in radio line probes of the early Universe in a unified manner. The program was designed to address the entire scope of relevant topics, ranging from what we know about potential foregrounds, to how to develop and demonstrate suitable technology for spectral observations, to unresolved theoretical

challenges of calculating line strengths and the evolution of source populations. Our motivation was to conduct a broad exploration, bringing together all of the pertinent information and practitioners in one place to look for exciting paths at the confluence of new technologies and theoretical expectations.

The Study Program considered technological and scientific exploration needed to study the first era of structure formation in the early Universe and to probe the interplay between dark matter and baryons at high redshift. The goal of our Study Program was to identify the most promising observational avenues to filling the missing history, and to provide a better understanding of the current technical and scientific roadblocks to progress and how to overcome them.

3

Components of the Study

Our Study Program was structured around the principal theme of diffuse spectral radio/mm/sub-mm observations that target atomic and molecular lines as tracers of large-scale structure and baryonic matter in the pregalactic and intergalactic medium. These lines and related scattering and spectral signatures are present during recombination in the form of highly redshifted atomic recombination lines of H and He, and at subsequent times as molecular cooling lines (from, e.g., CO, H_2), metal fine-structure forbidden lines, and the rest-frame 21 cm H I hyperfine line.

The structure of the Study Program was divided into two components based on observational and technological techniques: 1) large-beam spectral observations targeting primarily recombination-era atomic physics and probes of fundamental physics, and 2) small-beam tomography observations that would probe the Dark Ages, Cosmic Dawn, and the Epoch of Reionization. In addition, we scheduled a special session on spin-off scientific and technical opportunities, including new avenues to probe the forest of anomalous spinning dust lines or detect counterparts to diffuse optical bands in the ISM.

The organizing questions for each component were:

- What is the unique and compelling science?
  - Which features do we target?
  - What is the secondary science?
  - Are the desired measurements feasible and where are the limitations?
- What is the best approach to the desired measurements?
  - Monopole or anisotropies?
  - Ground, balloon, or space?
  - Calibration strategies
  - Analysis strategies (e.g., redshifted 21 cm techniques)
- What additional technology, analysis, or theory development is needed?

3.1 Outcomes of the Study

The Study Program identified two unique CMB spectral observations with the potential to yield extremely compelling scientific results that would significantly influence the study of the early Universe. The first of these is a long-term goal to measure **spectral line features from the recombination epoch**. Theoretically predicted recombination lines imprinted today as minute spectral deviations from the CMB blackbody spectrum due to hydrogen and helium recombination physics both at the time of the surface of last scattering and before could provide the earliest direct probes of the thermodynamic state and radiative processes immediately following the Big Bang. Measurement of these lines would provide the potential for game-changing discoveries by testing the dark matter annihilation in the redshift range $6000 > z > 1000$, and also by allowing a test of the time-dependence of the fine-structure constant at a critical epoch not accessible through other observations. In addition, recombination line measurements would test inflation models using an independent method through precision measurement of the spectral index of primordial perturbations, n_s. We discuss the recombination-line scientific objectives in more detail in Section 4.

The second key science observation identified by the Study Program is to adapt CMB anisotropy measurements to detect **large-scale structure during the reionization epoch** ($6 < z < 10$) using unresolved line emission from star-forming galaxies as a tracer of matter. These early eras of Cosmic Dawn and the Epoch of Reionization were identified as science frontier discovery areas by the recent New Worlds, New Horizons in Astronomy and Astrophysics Decadal Survey for the 2010 decade. The proposed observations would directly delineate the large-scale structure of the galaxies responsible for reionizing the Universe and provide the only foreseeable measurements on scales sufficiently large to compare with upcoming redshifted 21 cm observations of reionization. CO, [C II], and Ly-α lines were investigated as promising targets. CO and [C II] line transitions emerged as particularly compelling. Transition line maps would yield the inverse view of reionization from 21 cm maps, and together the two techniques would show the complete mechanics of reionization by illuminating the structure of both the sources of reionizing photons and the photon sinks in the IGM. This double view was deemed critical for confirming beyond doubt the "inside-out" growing bubble model of reionization. We discuss this observation in detail in Section 5.

The two science objectives identified in the Program share some common core technological requirements based on the shared need for approximately 1000 element feed arrays followed by broadband, high-resolution spectral correlators. The science drivers identified in the Study Program provide compelling roadmaps for development of large feed arrays beginning with applications in a ground-based CO mapping instrument and leading to a space-borne recombination-line all-sky spectrometer, and for development of a high-throughput multi-pixel spectroscopic instrument for mapping emssion from [C II]. Through these objectives, the Study Program provides strong motivation for a well-articulated and staged technology development program addressing the key technical issues including compact and light-weight integrated spectral dual-polarization inexpensive receiver modules, large high-resolution spectral correlators (analog and/or digital), and lightweight feeds. In parallel we recommend long-term investigations into high precision calibrators and calibration techniques that will be required for the recombination line instrument.

The technology program developed in the Study has synergy with the new era of large ground-based radio telescopes, including the science and technical pathfinding activities for the Square Kilometer Array (e.g., lightweight focal plane arrays, large correlators, as well as the LOFAR, MWA, and other redshifted 21 cm science objectives). In addition, we reiterate that the development of a CO-instrument receiver will be an excellent pathfinder for a recombination line instrument that could be realized in the 2020 decade.

4

Spectral lines from the cosmological recombination epoch

Since the early ideas (Zeldovich et al. 1968; Peebles 1968; Dubrovich 1975) on the existence of spectral distortions to the CMB blackbody generated during the cosmological recombination epoch ($z \sim 1400$ for hydrogen; $z \sim 2000$ for neutral helium, and $z \sim 6000$ for singly ionized helium), several theoretical studies have been pursued (for a more detailed overview, see Sunyaev and Chluba 2009). These studies considered different compelling scientific possibilities in connection with future observations of the cosmological recombination radiation. During this workshop we discussed the following questions:

- What can one actually learn by observing the cosmological recombination radiation?
- Is the motivation for such observations sufficient?
- Is it realistically possible to observe relic recombination lines?
- What are the main observational obstacles and steps towards the measurements?

In this section we summarize the particular outcomes of the workshop in each of these areas. We start by highlighting some of the results from earlier studies on the scientific opportunities in connection with the recombination radiation. We then outline a few possibilities for future theoretical investigations that could further motivate experimentalists to take on the challenging task to observe these recombination lines. Beyond any doubt it will be very hard to measure the distortions from the recombination epoch, but the discussions during the workshop have shown that it does not seem impossible to push open the window to observe these lines at some point in the future.

4.1 Information content of cosmological recombination features

Recent theoretical computations have shown that within the standard cosmological model it is possible to predict the spectral distortion coming from the recombination epoch with high precision, both for hydrogen

(Rubiño-Martín et al. 2006; Chluba and Sunyaev 2006) and helium (Chluba and Sunyaev 2009; Rubiño-Martín et al. 2008). As an example, in Figure 4.1, we show the recombination lines generated by hydrogen at redshift $z = 1300$–1400, which after redshifting should be visible at frequencies ranging from 100 MHz to a few THz today.

Because of the small number of baryons in the Universe these distortions to the CMB blackbody are tiny, with $\Delta I_\nu/I_\nu \sim 10^{-9}$ close to the maximum of the CMB blackbody ($\nu \sim 150$ GHz), and $\Delta I_\nu/I_\nu \sim 10^{-6}$ around 1 GHz (cf. Fig. 4.1), with variability of $\Delta T \sim \pm 1$–15 nK and typical width of spectral features $\Delta\nu/\nu \sim 10$–20% (see Figure 4.2).

Measuring the recombination lines will be a very challenging observational task, but such observations may allow us to open a very rich and interesting new window to *early Universe cosmology and fundamental physics*. In particular, the cosmological recombination lines should allow us to:

(i) *Improve determination of standard cosmological parameters,* most importantly, the baryon density, $\Omega_b h^2$, the abundance of helium, Y_p, and the temperature of the CMB monopole, T_0 (e.g., Chluba and Sunyaev 2008b). This could allow us to further narrow the constraints on cosmological parameters and help break degeneracies.

(ii) *Empirically test our understanding of the recombination dynamics,* a possibility that may become very important in connection with the final results from the *Planck* satellite. If $n_s < 1$ is found it will be extremely important to make sure it is not caused by an incomplete recombination model or unexpected processes during the recombination epoch.

These two points address the *safe* opportunities related to the cosmological recombination radiation: in case nothing *unexpected* happened during the early stages in the history of our Universe, it is clear that at the very least the cosmological recombination radiation should exist and should provide us a possibility to prove that the Universe was very simple at times *before* even last scattering at redshift $z \sim 1100$ (see Figure 4.3). In this case, the theoretical predictions of the recombination spectrum are limited by our understanding of atomic physics and detailed radiative transfer in a hydrogen-helium plasma. Here we mention that, in particular, refinements in connection with *collisional rates* may become important in the future.

However, if something *unexpected* occurred before the end of the recombination epoch (any time at $z > 800$), then the cosmological recombination spectrum could provide the unique opportunity to constrain non-standard extensions of the current cosmological model. It has been shown that the cosmological recombination radiation will be affected if:

(iii) *The CMB has intrinsic spectral distortion* (e.g., y- or μ-type, Illarionov and Siuniaev 1975), prior to the end of cosmological recombination. In this case *loops of transitions* lead to the production of photons by hydrogen and helium with the purpose of restoring full thermodynamic equilibrium (Lyubarsky and Sunyaev 1983; Chluba and Sunyaev 2008a).

(iv) Energy is injected into the primordial medium which directly ionizes hydrogen or helium atoms. Here possible changes to the recombination radiation from hydrogen caused by annihilating dark matter have been discussed (Chluba 2010).

In this context it is important that the recombination lines originate from three main stages in the thermal history of our Universe, all before the last scattering surface at which the CMB temperature and polarization anisotropies are formed (see Figure 4.3). This implies that the recombination lines may allow us to

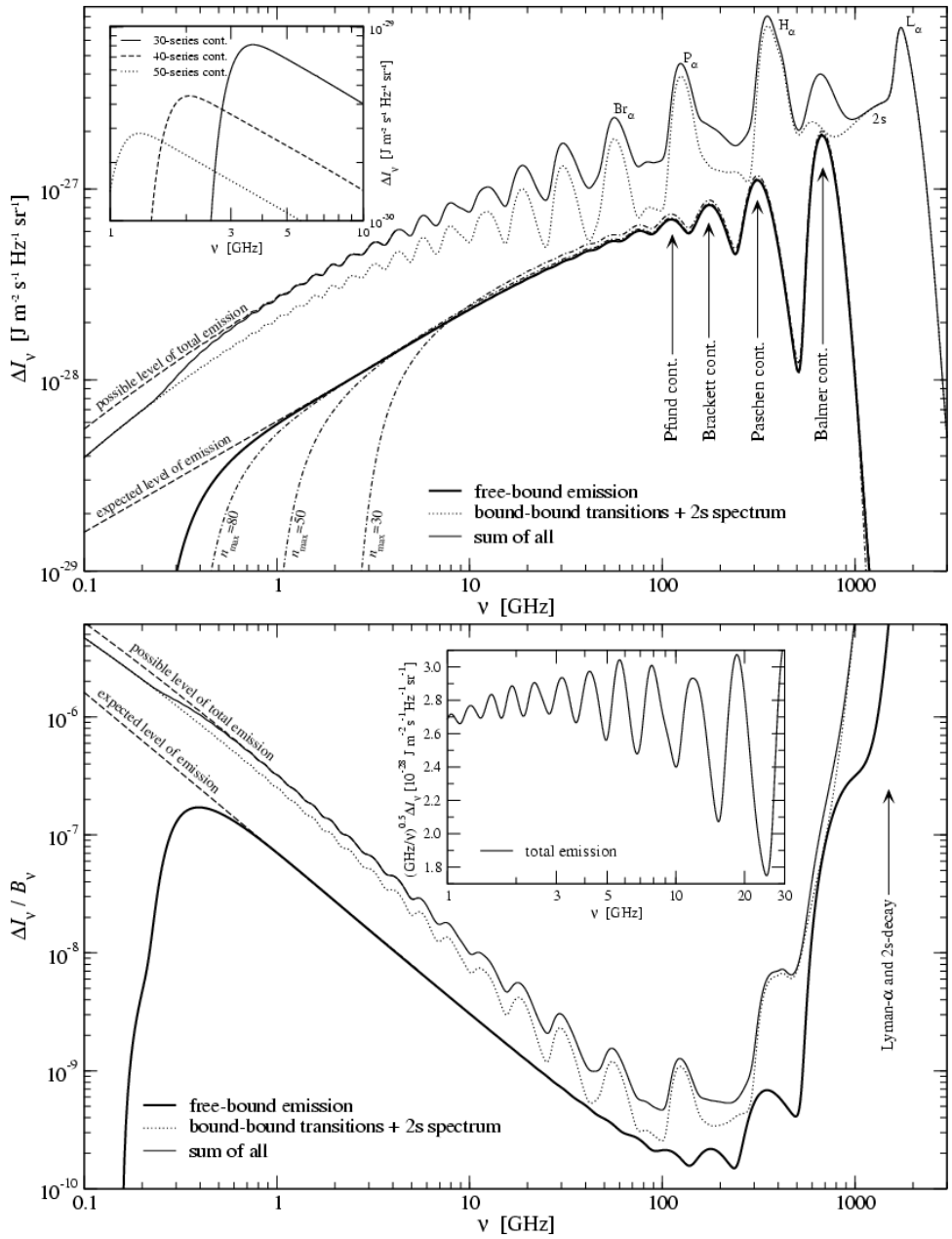

Figure 4.1: The hydrogen recombination spectrum including free-bound emission, from a computation for 100 shells. At high frequencies one can distinguish spectral features caused by different redshifted α-transitions. The width of these features is determined by the duration of the recombination process. The contribution due to the broad $2s$–$1s$ two-photon continuum is also included. The dashed lines at low frequencies indicate the expected level of emission when including more shells. Today computations with up to 350 l-resolved shells ($\sim 61\,000$ levels) are possible (Chluba et al. 2010). In the upper panel we also show the free-bound continuum spectrum for different values of $n_{\rm max}$ (dashed-dotted). The inlay gives the free-bound emission for $n = 30$, 40, and 50. The lower panel shows the distortion relative to the CMB blackbody spectrum, and the inlay illustrates the modulation of the total emission spectrum for $1\,{\rm GHz} \leq \nu \leq 30\,{\rm GHz}$ in convenient coordinates. [Figure from Chluba and Sunyaev 2006.]

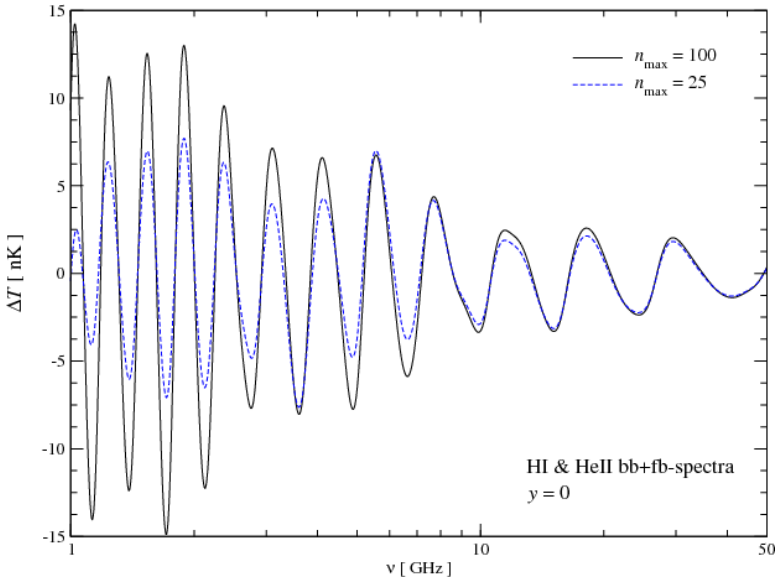

Figure 4.2: Frequency-dependent modulation of the CMB temperature caused by photons from the H I and He II recombination epochs. Both the bound-bound and free-bound contributions were included, and the mean recombination spectrum was subtracted. The signal is practically unpolarized and the same in all directions on the sky. [Figure from Chluba and Sunyaev 2009.]

constrain non-standard processes that may otherwise be unobservable in terms of the CMB anisotropies. One simple example is connected with point (iii): say in the future with a Firas II type experiment a y-distortion with $y \sim 10^{-6}$ is found, then this alone does not allow a very precise dating of the time at which the distortion was produced. It could have just originated as a consequence of structure formation at low redshift ($z = 1$–10), but have nothing to do with energy injection at high redshift because of some non-standard process. This is because a y-type distortion is rather featureless; however, the photons produced by atomic transitions in hydrogen and helium could eliminate this ambiguity (Chluba and Sunyaev 2008a).

4.2 Future theoretical investigations

Points (i)–(iv) mentioned in the previous section already demonstrate some of the interesting possibilities in connection with observations of the cosmological recombination radiation. As mentioned, (i)–(ii) are connected with the standard cosmological picture, and as such just provide possibilities for refinements and reassurance of our understanding of the Universe, while (iii)–(iv) push beyond the standard picture and indicate a potential new window to the early Universe.

There are additional possibilities, which have been mentioned in the literature before (Chluba 2010), but not previously worked out in detail. From the earlier studies discussed above it is clear that the cosmological recombination spectrum should in principle also be sensitive to:

(v) *Direct ionizations of hydrogen or helium atoms by decaying relic particles* (e.g., excited states of dark matter). If these decays end before hydrogen recombination, then the CMB anisotropies may not be affected at all, so that only the CMB energy spectrum could tell the tale about such processes.

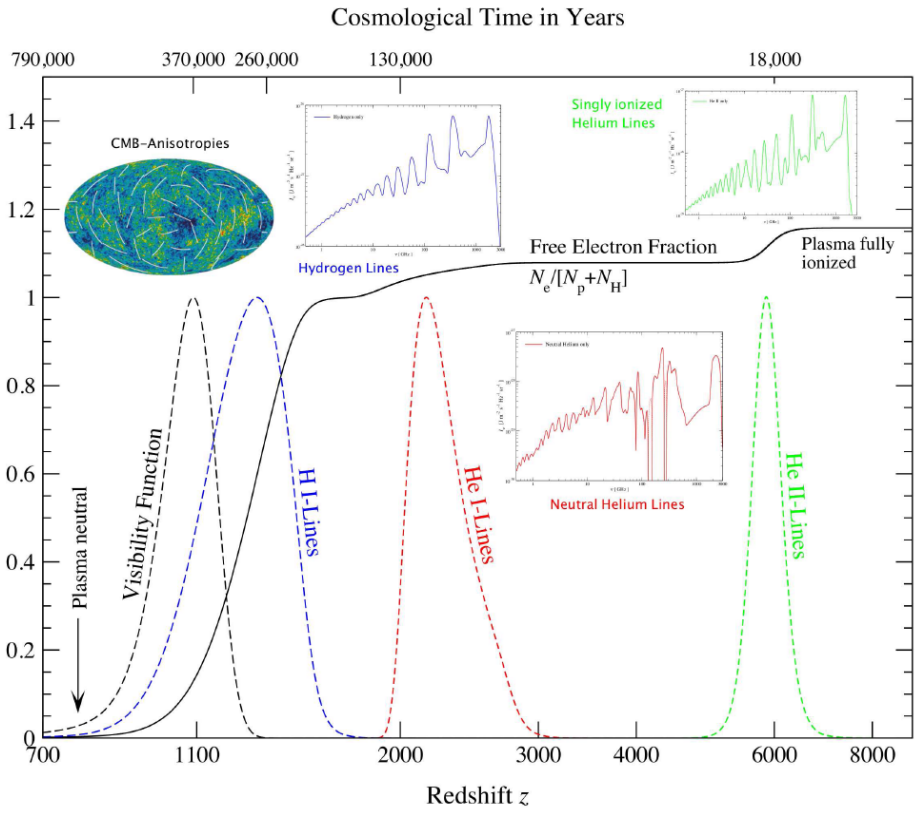

Figure 4.3: Ionization history of the Universe (solid black curve) and the origin of different CMB signals (dashed lines and inlays). The observed temperature anisotropies in the CMB temperature are created close to the maximum of the *Thomson visibility function* around $z \sim 1089$, whereas the direct information carried by the photons in the cosmological hydrogen recombination spectrum is from slightly earlier times. The photons associated with the *two* recombinations of helium were released at even higher redshifts. Finding the traces of these signals in the cosmological recombination spectrum will therefore allow us to learn about the state of the Universe at $\sim 130\,000$ years and $\sim 18\,000$ years after the big bang. Furthermore, the cosmological recombination radiation may offer a way to tell if something unexpected (e.g., energy release due to annihilating dark matter or decaying relict particles) occurred *before* the end of cosmological recombination. Also it may allow us to constrain variations of fundamental constants, such as the fine-structure constant or the electron and proton rest mass, over cosmological times. [Figure from Sunyaev and Chluba 2009.]

(vi) *Variations of fundamental constants*, such as the fine-structure constant α, or the electron and proton mass, m_e and m_p. Because of the direct dependence of the atomic processes (e.g., transition rates and frequencies) on these constant it is clear that this should affect the recombination lines, where the variations could potentially arise due to the presence of scalar fields that couple to the baryonic sector during the recombination epoch.

In connection with (v) it is most important to mention that the energy injection could be very small, so that it does not lead to any significant intrinsic *y*-type distortion (due to the huge number of CMB photons), but could still result in significant *reprocessing* of energy in the baryonic sector, leading to large changes of the recombination features. In future detailed calculations of this process, it will be important to account for the *branching* of the different decay products into *ionizations* and *excitations* of hydrogen and helium ions. Here one should also include the *double reprocessing* of He II photons by neutral helium and hydrogen, which in the standard recombination process leads to an enhancement of the number of recombination photons related to helium in the Universe (Chluba and Sunyaev 2009). Regarding point (vi), variations of α could in principle occur on time scales significantly shorter than the duration of recombination. This could lead to variations in the ionization history that cannot be constrained by precise measurements of the CMB anisotropy power spectra, but the corresponding changes in the spectral lines from recombination might be measurable. Furthermore, again because of the three different epochs during which the lines are formed, it will be possible to constrain such variations over cosmological periods of time. This would open a new independent window to fundamental physics, an opportunity that may become very interesting once new constraints on the Higgs boson are available from the Large Hadron Collider.

5

Intensity Mapping of the Cosmic Dawn

Cosmic reionization corresponds to the epoch when the neutral intergalactic medium (IGM) is reionized by light from the first galaxies (Barkana and Loeb 2005). This epoch, and the preceding "dark ages" between recombination and reionization, represents the *Universum Incognito*—the last unexplored epoch of cosmic structure formation. Current observational constraints, based primarily on large scale polarization of the CMB and Lyman-α scattering of light from $z > 6$ quasars (the Gunn–Peterson effect), suggest that reionization may have had a large variance in space and time, starting at $z \sim 14$, and extending down to $z \sim 7$ (Fan et al. 2006). The most direct advances in the study of cosmic reionization will come through observations of the H I 21 cm emission from the neutral IGM. Extensive theoretical and observational work is on-going to study the H I 21 cm signal from the neutral IGM during cosmic reionization, into the preceding dark ages (Furlanetto et al. 2006; Morales and Wyithe 2010). But that is only one side of the picture: we also need to study the reionizing sources—galaxies—in detail.

One of the key science programs that emerged during the KISS workshop is the possibility of studying the large-scale distribution of galaxies (scales $> 100\,\mathrm{deg}^2$) during reionization through "intensity mapping" of the emission from molecular, atomic, or ionized gas in star forming galaxies at $z > 6$. Tracing the distribution of the galaxies that reionize the Universe is the complementary diagnostic to the H I 21 cm studies of the earliest epochs of galaxy formation (see Figure 5.1). Indeed, a cross correlation between the large-scale structure of star forming galaxies, and the structure of the neutral IGM, will provide a comprehensive, model-independent view of universal evolution during the epoch of first light. Relative to each other, these two probes provide critical "inverse views" of the Universe.

Figure 5.2 illustrates the intensity of several line species relative to the star formation rate. After consideration of observational feasibility, three species emerged as offering particularly promising probes of the high-redshift Universe; they are potentially quite strong emission lines and probe complementary phases of the interstellar media of these early galaxies. First, CO transition lines (with rest frequencies at 115 GHz and 230 GHz for the lowest two transitions) are an extremely important probe of highly molecular gas in the nearby Universe, and there is a tight correlation between star formation rate and CO luminosity. Second, the [C II] transition of singly-ionized carbon, C^+, at $158\,\mu$m is the most important coolant for

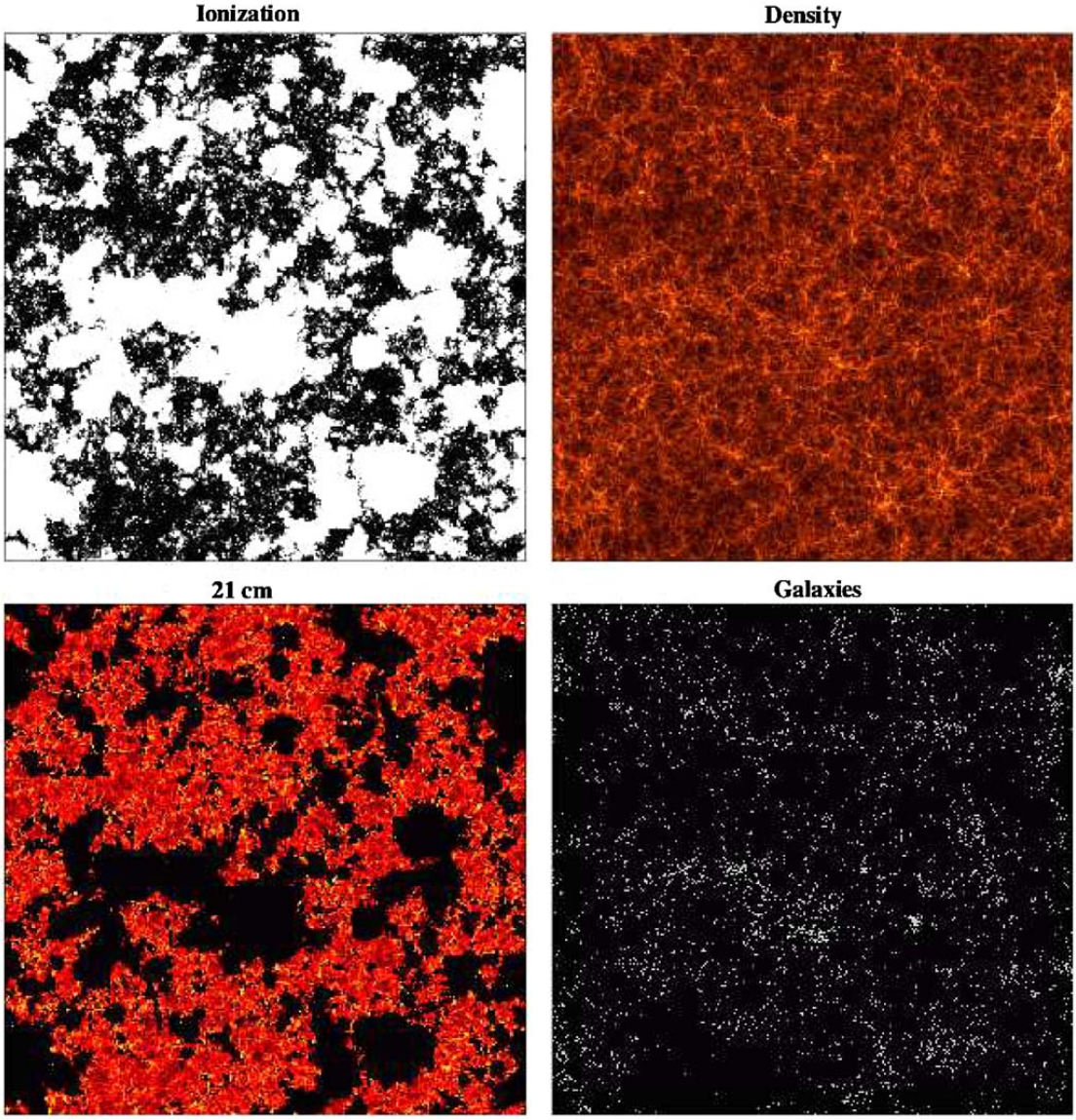

Figure 5.1: Simulated maps of the density, halo, ionization, and 21 cm fields. Each map is 130 Mpc$/h$ on a side and is drawn from a simulation snapshot at $z = 7.32$ at which point $\langle x_i \rangle = 0.54$. The density, ionization, and 21 cm maps are each 1 cell thick (0.25 Mpc/h), while the halo field is from a 60-cell (15 Mpc$/h$) wedge. On large scales, the bright regions in the overdensity map tend to have more halos, be ionized, and be dim in 21 cm. The correspondence between the bright regions in the halo field, and the dim regions in the 21 cm field, is the signal that a CO mapping instrument would aim to constrain [Figure from Lidz et al. 2009].

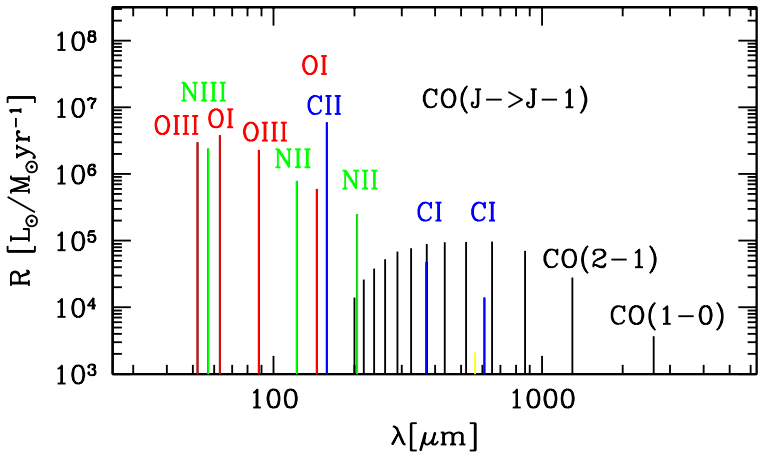

Figure 5.2: Ratio between line luminosity, L, and star formation rate, $\dot{M}_*$, for various lines observed in galaxies and taken from Table 1 of Visbal et al. (2011). For the first seven lines this ratio is measured from a sample of low redshift galaxies. The other lines have been calibrated based on the galaxy M82. Some weaker lines, for example for HCN, have been omitted for clarity [Figure from Pritchard and Loeb 2011].

warm neutral gas, and it can contain nearly 1% of the bolometric luminosity of a nearby galaxy. Finally, $\sim 2/3$ of hydrogen recombinations in ionized gas produce Lyman-α photons. These three species therefore probe molecular, atomic, and ionized gas, and together they can potentially provide a powerful picture of the interstellar media of galaxies during the cosmic dawn.

The most obvious way to use these lines is to measure the emission properties of individual galaxies. In the near future, the Atacama Large Millimeter/submillimeter Array (ALMA) and the Expanded Very Large Array (EVLA) will be able to detect the CO and [C II] emission from individual, massive galaxies at $z > 6$ (see Wang et al. 2011, and references therein). Such studies will be crucial to obtain an unbiased picture of the molecular gas content of high-redshift galaxies and its physical properties (through CO dynamics, morphology, and excitation), its relation to atomic gas reservoirs (through [C II] measurements) and to determine the relative contributions of different galaxy populations to reionization. Meanwhile, near-infrared surveys are already detecting hundreds of Lyman-α emitting galaxies at $z > 6$.

These instruments are likely to study "ultradeep fields" in order to find distant galaxies and map their properties in detail, which would require ~ 1000 h per observatory. However, the fields of view of these instruments are so small (< 1 arcmin) that "blind" searches for faint galaxies will be extremely difficult. Given that the typical mass scale of galaxies declines rapidly with redshift, and that intrinsically faint galaxies appear to dominate the reionization process, probing deeper down the luminosity function is a critical effort.

Moreover, such surveys—which are similar in spirit and scale to near-infrared galaxy surveys, such as those made with the *Hubble Space Telescope*—are difficult to compare to H I maps because of a severe mismatch in scale: the latter have resolutions of several arcminutes at best, about the same size as a deep galaxy survey. The comparison between the two is very powerful—revealing where the ionized gas is relative to galaxies is an extremely powerful probe of the reionization process. This requires a large-scale "galaxy survey" that probes deep down the luminosity function.

Such a survey is useful for a second reason as well. The H I 21 cm experiments are probing scales

ranging from 100 deg^2 to 1000 deg^2, over redshift ranges from $z \sim 6$ to 10, and have very coarse resolution (~ 10 comoving Mpc—comparable to the entire field of view of a large near-infrared telescope). Thus it is difficult to compare traditional galaxy surveys to the future H I experiments, even though such a comparison is extremely useful for understanding how these sources reionized the Universe.

The contrasting goals of depth and survey area are typically seen as mutually exclusive—and that is certainly the case for any survey than aims to resolve galaxies. A key result of the KISS workshop was to challenge this conventional wisdom with the emerging strategy of intensity mapping: treating the cumulative galaxy emission as a diffuse background that can be mapped relatively easily (with small telescopes) without resolving individual galaxies. Because the cumulative emission is likely to be dominated by faint sources, this technique is sensitive to these faint galaxies (although one only learns about them in aggregate), and because the survey scales are large they are well-matched to the H I surveys.

Moreover, by mapping out line emission from these galaxies, one can use the observed frequency of the line as a proxy for radial distance (through the cosmological redshift). Thus, a single measurement generates a tomographic map of the galaxy distribution, with three-dimensional information. This technique has already been demonstrated using the H I 21 cm line out to $z \sim 1$ Chang et al. (2010). In the following sections, we review the science case and the design parameters for high-redshift mapping instruments for CO (§ 5.1), [C II] (§ 5.2), Lyman-α (§ 5.3), and other species (§ 5.4).

5.1 Intensity mapping with CO

5.1.1 Science Goals

A direct outcome of our KISS study was a suite of calculations of the expected CO brightness on large scales from the galaxies that reionize the Universe. We have performed both analytic and numerical calculations in order to estimate the strength of the signal, and hence whether the technique is plausible (Carilli 2011; Gong et al. 2011; Lidz et al. 2011).

The redshifts of most interest are $z \sim 6$–10, which corresponds to observing frequencies of 21–33 GHz for CO (J=2–1) and 10–16 GHz for CO (J=1–0). Figure 5.3 illustrates the CO line transition frequencies as a function of redshift. The angular scales probed should be large enough to be easily observed and ideally also matched to the H I 21 cm experiments, which typically have resolutions of 5–10 arcmin, and fields of view 5–40 deg (FWHM).

The simplest approach to calculate the CO signal from star forming galaxies during reionization is to assume that local relationships between the star formation rate and CO luminosity hold in these early galaxies and to calibrate the total star formation rate density to that required to maintain reionization. Carilli (2011) shows that the mean CO brightness temperature at $z = 8$ will then be $\langle T_B \rangle = 1.1(0.1/f_{\rm esc})(C/5)\,\mu$K, where $f_{\rm esc}$ is the escape fraction of UV photons from the first galaxies, and C is the IGM clumping factor. This base estimate is uncertain by a factor of a few, but it provides a rough guide for the mean signal (see also Gong et al. 2011; Lidz et al. 2011).

However, theoretical predictions of the actual signal are uncertain by a much larger factor, because the physics of CO emission is not very well understood. This estimate relies on the local conversion of star formation rate to CO luminosity, which is poorly understood theoretically. There is some evidence that the CO luminosity declines rapidly with galaxy metallicity, although whether the low-metallicity galaxies in which this occurs are good analogs for high-redshift star-forming galaxies is questionable. CO has been detected from massive galaxies at $z \sim 6$ (Wang et al. 2011). It is therefore very important to measure how

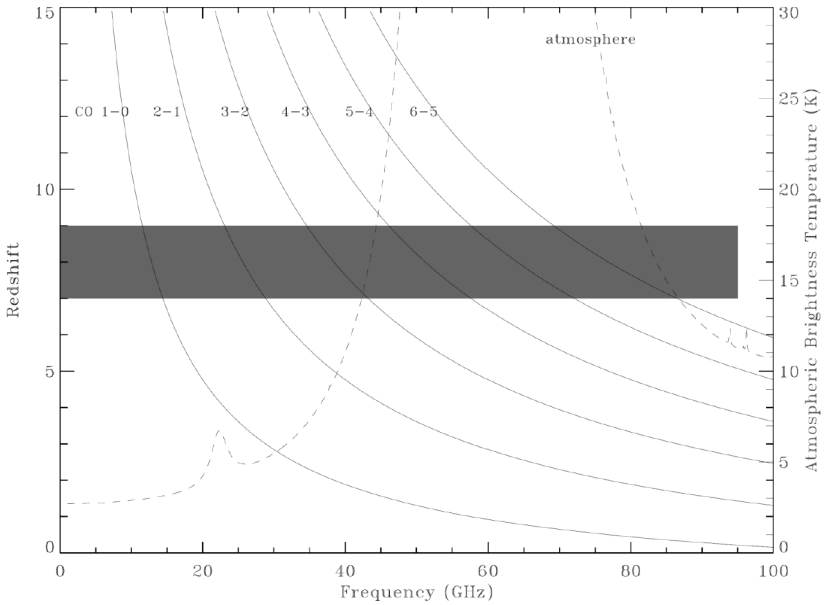

Figure 5.3: Relationship between redshift and observed CO line transition frequencies. Atmospheric brightness temperature is shown by the dashed line. From the ground, the atmosphere will significantly hinder observations above about 50 GHz.

the CO luminosity does evolve—from the nearby Universe to the cosmic dawn—in order to understand the history of star formation.

Intensity mapping is not sensitive to this mean signal but rather to fluctuations with either angle (on the plane of the sky) or frequency (which can be mapped to distance in the radial dimension, because we are observing a line). Lidz et al. (2011) and Gong et al. (2011) have used large-scale numerical simulations of the reionization process to estimate the expected CO brightness temperature and its fluctuations due to large-scale structure during reionization. The amplitude of these fluctuations depends upon the scale studied, but (if local relations hold) they are typically ~ 0.1–$1\,\mu$K for the angular and frequency scales of interest to us.

Is it plausible to detect such a signal? Without going into detailed instrument design, we simply consider receiver noise and brightness temperature. For a 20 K receiver system in 1000 hours and a 130 MHz channel (= 1500 km s^{-1} at 26 GHz, corresponding to 5 arcmin in angle, or a cube of 133 Mpc^3), the standard radiometer equation yields $\delta T = 0.9\,\mu$K. Hence, achieving a 1σ brightness sensitivity per pixel is plausible in a long integration. Note that an angle of 5 arcmin at 26 GHz corresponds to the diffraction-limited beam of an 8 m antenna.

However, because intensity-mapping experiments do not resolve individual galaxies, it is natural to treat these experiments statistically anyway. In that case, the large fields of view enable one to measure the properties of huge sets of pixels and produce key physical constraints even when the noise per pixel is of order unity (or even smaller).

Moreover, for the foreseeable future the H I experiments will also be in this low signal-to-noise per pixel regime, at least on moderate scales, so a comparison with them must be statistical. Nevertheless, this can be extremely powerful. Theoretical models predict that the reionization process is "inside-out," or that

it begins in large-scale overdense regions (with many luminous sources) and then proceeds to large-scale underdense regions. If so, we would expect an *anticorrelation* between CO emission and H I emission: the CO signal, from galaxies, would be centered in large-scale overdense regions. Measuring this requires separate tracers of galaxies and H I.

However, on small scales the two would be uncorrelated, because galaxies ionize a large region around themselves. The crossover between these two regimes would then provide the typical scale of ionized regions, something that is also difficult to measure in a model-independent way from the H I emission alone.

During the KISS workshop, we identified the following key science goals for such a measurement:

1. Measure the power spectrum of CO emission as a function of redshift. This depends on the clustering of the galaxies hosting CO emission (and hence the mass of these galaxies) and the relation between CO luminosity and star formation. Mapping how this relation evolves with redshift, from $z \sim 2$ to $z \sim 10$, would provide a powerful window into the history of star formation, though detailed conclusions are degenerate between these two parameters. The comparison with other probes, like multiple CO lines, [C II], and Lyman-α, will also teach us a great deal about the internal physics of galaxies.

2. Measure the cumulative cross-correlation between CO and H I emission on large scales. This would test the "inside-out" picture of reionization.

3. Measure the cross-correlation between CO and H I emission as a function of physical scale and redshift, which will constrain the typical size of ionized regions during reionization. This scale is likely to correspond to a few arcminutes and so requires relatively good angular resolution (though note that the relationship between observed frequency and distance enables us to probe to somewhat smaller physical scales than the nominal angular resolution of a telescope).

4. Break the degeneracy between clustering (and hence typical galaxy mass) and CO luminosity per unit star formation by either (1) measuring the shape of the CO power spectrum on small scales or (2) measuring the *redshift-space* distortions in the CO power spectrum, or the asymmetry between radial distance and distance on the plane of the sky. The former depends on the velocity field, which allows one to measure the clustering strength independently.

Of course, these measurements are far from easy. A particular challenge is ensuring that one is observing the CO line of interest rather than contamination from other continuum or line foregrounds (such as lower CO transitions at lower redshifts). Cross-correlation is a powerful tool to remove line contamination; i.e., comparing the CO(1–0) and CO(2–1) emission from a single redshift slice will isolate the CO emission. Cross-correlation with another galaxy survey (which may be useful at lower redshifts) or with the H I emission, can accomplish a similar goal.

5.1.2 Foregrounds and secondary astrophysics

Recent CMB experiments have greatly improved our knowledge of the foreground properties in the cm and mm bands. Galactic synchrotron and dust emission are primary foregrounds (e.g., Figure 5.4), along with extragalactic point sources. However, at the sub-microkelvin level sensitivities and high spectral resolutions required for the CO experiments, our empirical foreground knowledge is limited and the standard

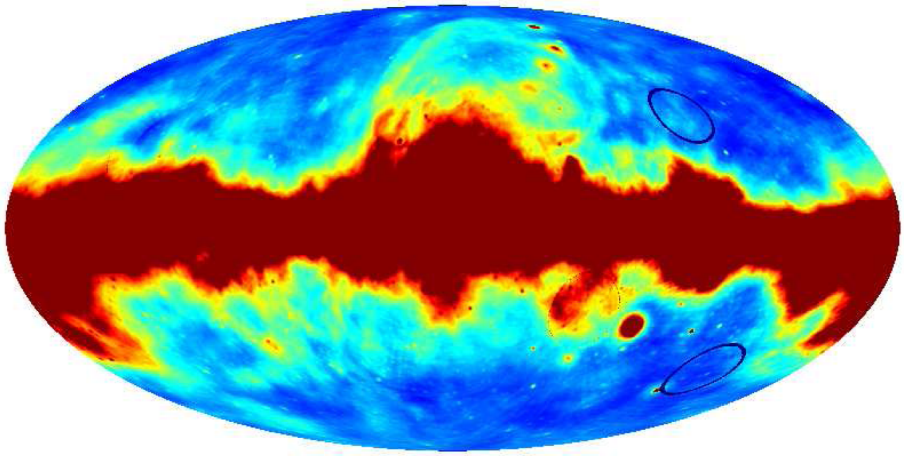

Figure 5.4: Map of the sky temperature at 25 GHz predicted by the GSM model. The color scale varies from 0 to 250 μK. The two black 10° radius circles at the positions $(l,b) = (228°, -49°)$ and $(253°, 38°)$ are centered on the MWA primary and secondary observing regions, respectively.

techniques for foreground removal employed by traditional CMB studies are insufficient. In principle, each of the foreground sources has a very smooth spectrum, so it should be possible to subtract them from tomographic CO intensity maps using the same techniques planned (and soon to be demonstrated) for 21 cm observations.

Spinning Dust

Microwave emission from dust is both a key secondary science opportunity and an important foreground that may strongly contaminate the CMB spectral studies unless it is accounted for. At high frequencies (> 100 GHz) the main contamination comes from vibrational dust emission, while at lower frequencies ($15 \leq \nu \leq 60$ GHz) it may come from another dust population composed basically of small grains that emit radiation via rotational rather than vibrational excitations (Draine & Lazarian 1998). The "anomalous" small grain component is spatially correlated with the 100 μm dust emission but with a spectrum that rises towards lower frequencies, subsequently flattening and turning down somewhere around 15 GHz (see de Oliveira-Costa et al. 2004, Gold et al. 2010).

The rotational emission from extremely small dust particles consisting of polycyclic aromatic hydrocarbons (PAHs) is potentially one of the dominant Galactic foregrounds at frequencies from $\sim$ 5–30 GHz. The observed spectrum is believed to be the superposition of spectra of several types of PAHs, with various excitation degrees, and various rotational constants. The resulting forest of rotational lines could, due to its discrete nature, therefore lead to non-smooth features when convolved with a finite bandwidth (see Figure 5.5). Although usually modeled as a continuum, the spinning dust foreground is, therefore, a picket fence emission spectrum originating from each molecule. A simple model suggests structure will be at the microkelvin level.

For a single PAH species, the amplitude of the fluctuations is simply given by the ratio of the line separation to the instrument bandwidth. When several species are present, the superposition of many lines will decrease the amplitude of the fluctuations. As an example, coronene ($C_{24}H_{12}$) has rotational constants

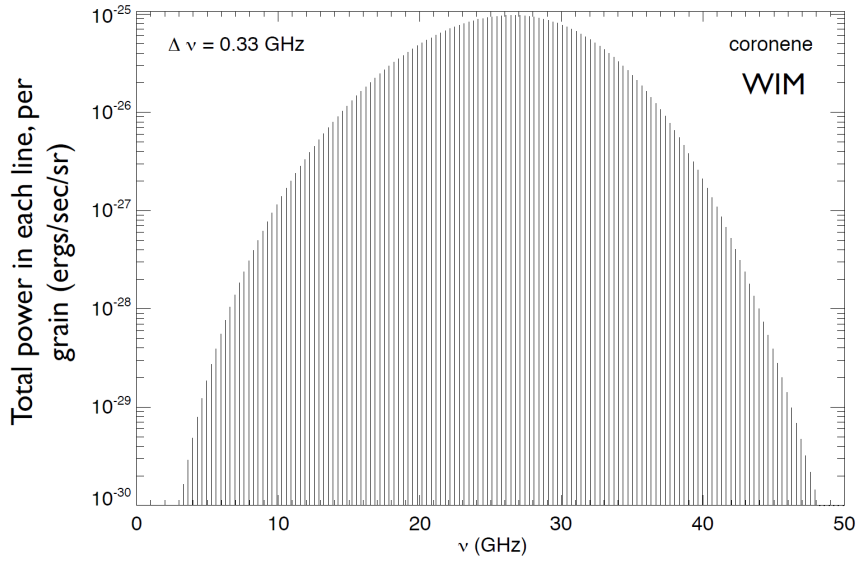

Figure 5.5: Theoretical model of the "forest" of discrete spectral lines that constitute the spinning dust model for anomalous microwave emission. An instrument designed for redshift CO spectral mapping would be able to validate this model by detecting individual spectral lines.

of 150 MHz and 300 MHz; circumcoronene ($C_{54}H_{18}$) has rotational constants of 33 MHz and 66 MHz. The total amplitude (not that of fluctuations) of the galactic spinning dust emission can be estimated to be of the order 0.1–1 mK. The question is therefore whether the relative amplitude of fluctuations when convolving with a finite bandwidth can be as low as 0.1% (for the CO line observation) or less than 1 part in 10^4 for the observation of spectral lines from the recombination epoch.

There is currently no "smoking-gun" demonstration that spinning dust radiation is the origin of the "anomalous" emission – other origins could be dust-correlated free-free or magnetic dust emission. Casting doubt on the spinning dust interpretation is that the spectral index of observed emission often does not match theory. Existing observations divide into two categories: detection of an anomalous foreground through spatial correlations of mid-IR and radio in the diffuse ISM, or spectral measurements in individual nebulae. No direct spectral measurement has been done in the diffuse ISM. Furthermore, the mid-IR lines ($\sim$ 3–12 μm) reflect the nearest-neighbor vibrations of PAHs and do not carry information about individual molecules.

PAHs are crucial constituents of the ISM: they contribute to the heating of the gas, and to the ionization balance, both of which are important for star formation. There is currently no consensus on which PAHs exist in the ISM or their properties (such as whether they are dehydrogenated, super-hydrogenated, etc.). Observing the rotational lines from PAHs, either in emission, or in absorption against strong background radio sources, could provide the missing information about these crucial constituents of the ISM. Hence, mapping PAH lines could in principle also give an additional window on the physical conditions in the ISM.

The open questions that could be addressed as secondary science by a CO intensity mapping instrument are: Is anomalous emission spinning dust? If not, what is it? Are there legitimate large-scale correlations? (A CO mapping instrument could cover a full hemisphere in $\sim$ 1 year to produce a good correlation map.) How many individual molecules contribute to the observed spectrum? How important is substitution?

And from a theoretical perspective, the Study Program brought attention to the question: Should the picket-fence structure already have been observed if it is there?

It was also noted during the Study Program, that if polarized emission were measured by a CO intensity mapping instrument, resonance in the magnetic dust spectrum (possibly in the 15–30 GHz range) could cause the polarization vector to flip, providing a strong signature to confirm or rule out the magnetic dust origin hypothesis. The potential for leveraging a polarized survey at 15–30 GHz with upcoming 5 GHz CBASS observations was identified as a particularly interesting source of secondary science in this regime.

In the near-term, we determined it would be valuable to:

- Evaluate the "bumpiness" of the spinning dust spectrum measured with a finite bandwidth, and the level of noise that this would induce for CO/Recombination line observations.
- Evaluate what information can be extracted from these observations about the PAHs existing in the ISM.
- Evaluate the optical depth for spinning dust absorption against background radio sources. If feasible, the EVLA could be used to acquire a spectrum toward bright quasar to search for spectral fluctuations in the absorption counterpart to anomalous emission.
- Evaluate at what level Galactic molecular and recombination lines produced strongly in the plane are scattered back to the Earth from diffuse gas at high Galactic latitudes.

Transients and Gravitational Wave Counterparts

The technical capabilities of a CO intensity mapping telescope would also enable time domain astronomy, in a program that could operate concurrently with the CO intensity mapping. One class of radio transients is the result of an explosive event in which an expanding fireball interacts with a surrounding medium, accelerating particles, and producing synchrotron radio emission. The peak flux density and frequency depends upon the characteristics of the surrounding medium, but the emission peaks at relatively high frequencies (> 10 GHz) and then shifts to lower frequencies (~ 1 GHz) over a period of days to weeks as the radio photosphere (or surface of unity optical depth) expands. The prototypical such source is a radio supernova, but more recently it has been recognized that gamma-ray burst (GRB) afterglows show a similar behavior in the radio. The sources may also represent an electromagnetic counterpart to gravitational wave (GW) events to be detected by the Advanced Laser Interferometric Gravitational Observatory (Advanced LIGO) or similar ground-based laser interferometric gravitational wave telescopes.

The proposed wide-field CO intensity mapping telescope would enable a new observational approach to finding such sources. The traditional approach has been to identify such sources in the optical, as their luminosities tend to peak first in the optical before shifting to longer wavelengths. However, this approach introduces a serious selection bias in that dust obscuration can "hide" the optical source, whereas radio wavelengths penetrate dust with little or no obscuration. Thus, one could begin to conduct effective searches for "dark" supernovae or GRB afterglows. Further, Advanced LIGO is likely to provide an initial uncertainty on the position of a GW event that is tens of degrees in size, requiring rapid wide-field mapping capabilities to search for possible radio wavelength counterparts.

Both time domain astronomy and gravitational wave astronomy were identified as science frontier discovery areas by the recent New Worlds, New Horizons in Astronomy & Astrophysics Decadal Survey.

5.2 Intensity mapping with [C II]

A complement to CO is the 158-μm fine-structure transition of ionized carbon, [C II]. Carbon is the fourth most abundant element in the Universe, and with an ionization potential substantially less than that of H, it is an important constituent in both neutral and ionized gas phases. The ground electronic state of C^+ has a fine-structure doublet, separated by 91 K, producing the 158-μm spectral line (hereafter [C II]). The transition is easily thermalized for typical conditions in galaxies, with critical densities of 3000 H_2 cm^{-3} in neutral gas, and 50 e^- cm^{-3} in ionized gas. These properties make [C II] one of the most important gas coolants in galaxies as a whole; empirically, the transition carries a fraction 3×10^{-4} to 10^{-2} of the total bolometric energy in galaxies, typically more than all of the CO transitions combined.

Much of the [C II] emission arises in regions where the stellar UV impinges upon molecular clouds, known as photo-dissociation regions (PDRs), shown schematically in Figure 5.6. Outside of the hydrogen-ionized (H II) region, UV photons with $E < 13.6$ eV penetrate into the molecular cloud, ionizing carbon to a depth limited by dust absorption of the UV (see Tielens and Hollenbach 1985), typically corresponding to a few magnitudes of extinction. The region over which the C^+ exists is the region in which the bulk of the stellar energy is deposited into the interstellar material; as a fraction of the total, about 1% heats the gas, the bulk going to the dust and emerging as far-IR continuum. At larger depth into the cloud, the recombination rate exceeds the ionization rate, and neutral carbon and ultimately CO become the dominant carbon repositories. In this model, a lower dust-to-gas ratio will result in increased C^+ fractional luminosity, and this is the leading explanation for the enhanced [C II] observed in low-metallicity dwarf galaxies in the local Universe (e.g., Madden et al. 2011). Figure 5.7 summarizes the [C II] observations in various classes of galaxies, and the relationship to the total bolometric luminosity and the CO emission. To the extent that the galaxies responsible for reionization resemble today's low-metallicity dwarfs, these considerations suggest that the [C II] emission may be enhanced relative to both CO and the total bolometric luminosity.

The CCAT submillimeter telescope will be a leading instrument for [C II] observations of discrete targets and we considered whether large-area intensity mapping might be possible with CCAT. The 1σ, $R = 1000$ spectral line sensitivity of CCAT is projected to be approximately 6 mK for a 1 s observation,[1] although this is for a non-heterodyne receiver. To reach 1 μK, therefore, would require over 10,000 h of integration. The field of view of a single CCAT feed at ~ 210 GHz will be approximately 15 arcsec. In order to cover 100 deg^2, therefore, CCAT would require ten million (diffraction limited) pixels. While large focal arrays are under development for CCAT, none is capable of reaching ten million elements in the foreseeable future. Moreover, the bandwidth for each feed is typically about 8 GHz with current correlator technology. This corresponds to a redshift interval of $dz = 0.34$ at $z = 8$, which is much less than the redshifted 21 cm experiments (which have $dz > 2$) and, therefore, poorly matched to provide high signal-to-noise statistical measurements. Increasing the spectral bandwidth of each feed to 32 GHz would be required to approach parity with the 21 cm redshift measurements.

Gong et al. (2012) have studied the potential for detecting [C II] emission from galaxies in the reionization epoch. As with CO, the individual galaxies are too faint to detect in sufficient numbers to be meaningful, but the aggregate emission can be measured in a wide-field spatial-spectral survey. The first step is to calculate the expected mean intensity in [C II] on the sky as a function of redshift. Gong et al. solve the C^+ level populations including collisional and radiative terms under various assumptions about metal fraction and gas density and temperature. The calculation, along with the sensitivity estimate are

[1] http://wiki.astro.cornell.edu/ccat

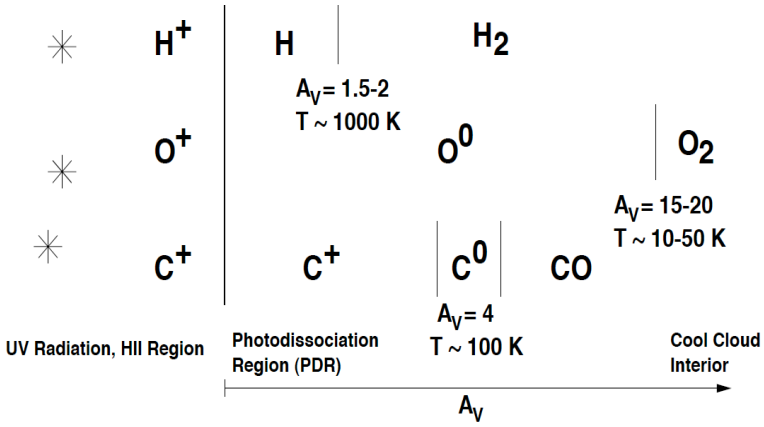

Figure 5.6: Photo-dissociation region (PDR) schematic showing the main features of the standard plane-parallel model originally developed by Tielens and Hollenbach (1985). [C II] is the primary gas coolant for the material between the H II region and the interior of the molecular cloud. For this standard mode, the gas density is 2.3×10^5 H cm^{-3}, and the UV field is 10^5 times the local interstellar radiation field. A_V is the V-band extinction into the cloud due to dust, measured in magnitudes. Temperatures refer to the gas; the run of dust temperature is much flatter, approximately uniform at 100 K.

shown in Figure 5.8. These first-principles calculations produce estimates similar to what is obtained in considering the current estimates of the co-moving star-formation rate history by a factor $\sim 10^{-3}$, the [C II] fractional luminosity.

As with the CO and H I, the [C II] from reionization-era galaxies is best interpreted through an auto-correlation power-spectrum, or via cross-correlation with the other tracers such as CO or H I. Figure 5.9 shows the auto-correlation power spectra and uncertainties that might be achieved using the strawman [C II] tomography instrument described in Section 6.3. As with CO, the cross-correlation with H I is expected to be negative for small k values, as the galaxies which are reionizing the medium are anticorrelated with the neutral inter-galactic medium. However, at $k \sim 1$ (corresponding to 2.5 arcmin angular scale and ~ 800 kpc physical scale at $z = 1$) this correlation becomes slightly positive, as shown in Figure 5.10. This relationship provides information about the size-scale of the individual bubbles and, if measured at various epochs, their evolution.

5.3 Lyman-alpha intensity mapping

Hydrogen recombination line emission, most prominently Ly-α emission, offers a potentially powerful probe for tomographic line mapping of the epoch of reionization. As shown in Figure 5.11, the spectrum of a massive Population-III star produces a continuum of hard UV photons. These are absorbed above the Lyman cutoff by the neutral intergalactic medium. The ionized region surrounding young galaxies also produces Ly-α line emission and free-free emission, and a large fraction of ionizing photons produce Ly-α line emission from e-p recombinations, as well as Ly-α emission from collisional excitation from free electrons in partially ionized gas. The Ly-α line is optically thick, so the intensity of the line depends on the escape fraction before other emission branches carry away radiant energy. We note that the general production of Ly-α photons is associated with the reionization of the intergalactic medium, whether the

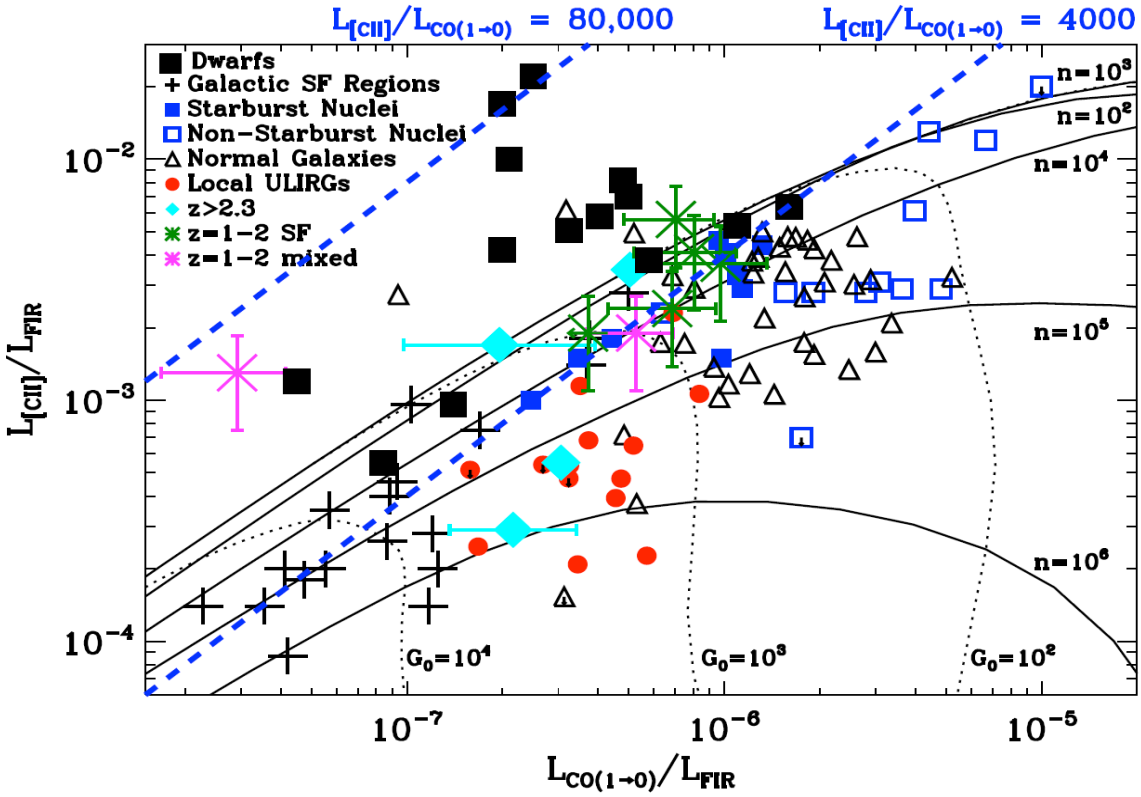

Figure 5.7: Fractional luminosities of [C II] and CO (J=1–0) observed in galaxies. The dwarf galaxies in the upper left are from the Madden et al. (2011) sample, and have metallicity ranging from 1/30 to 1/3 solar. The other points in the plot are from Stacey et al. (2010).

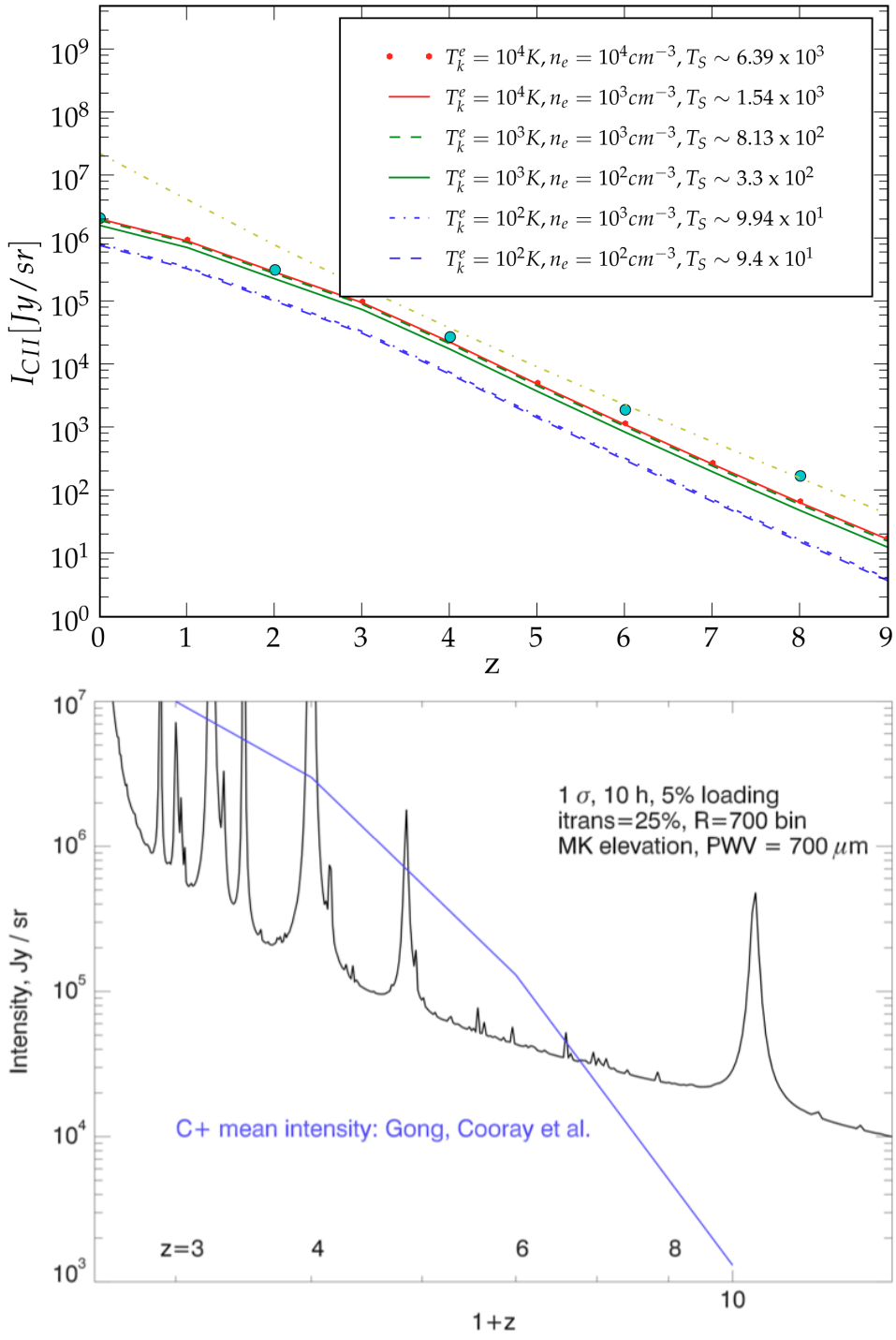

Figure 5.8: (*Top)* The mean intensity of [C II] emission line from the outputs obtained from the De Lucia and Blaizot (2007) simulation at several different redshifts. The yellow dotted line is the Gong et al. (2012) analytic result, and the blue spots are obtained from the simulation with the hot and warm gas contributing to the [C II] luminosity. (*Bottom*) This intensity overlaid with the sensitivity of a background-limited spectrometer on a mountaintop site.

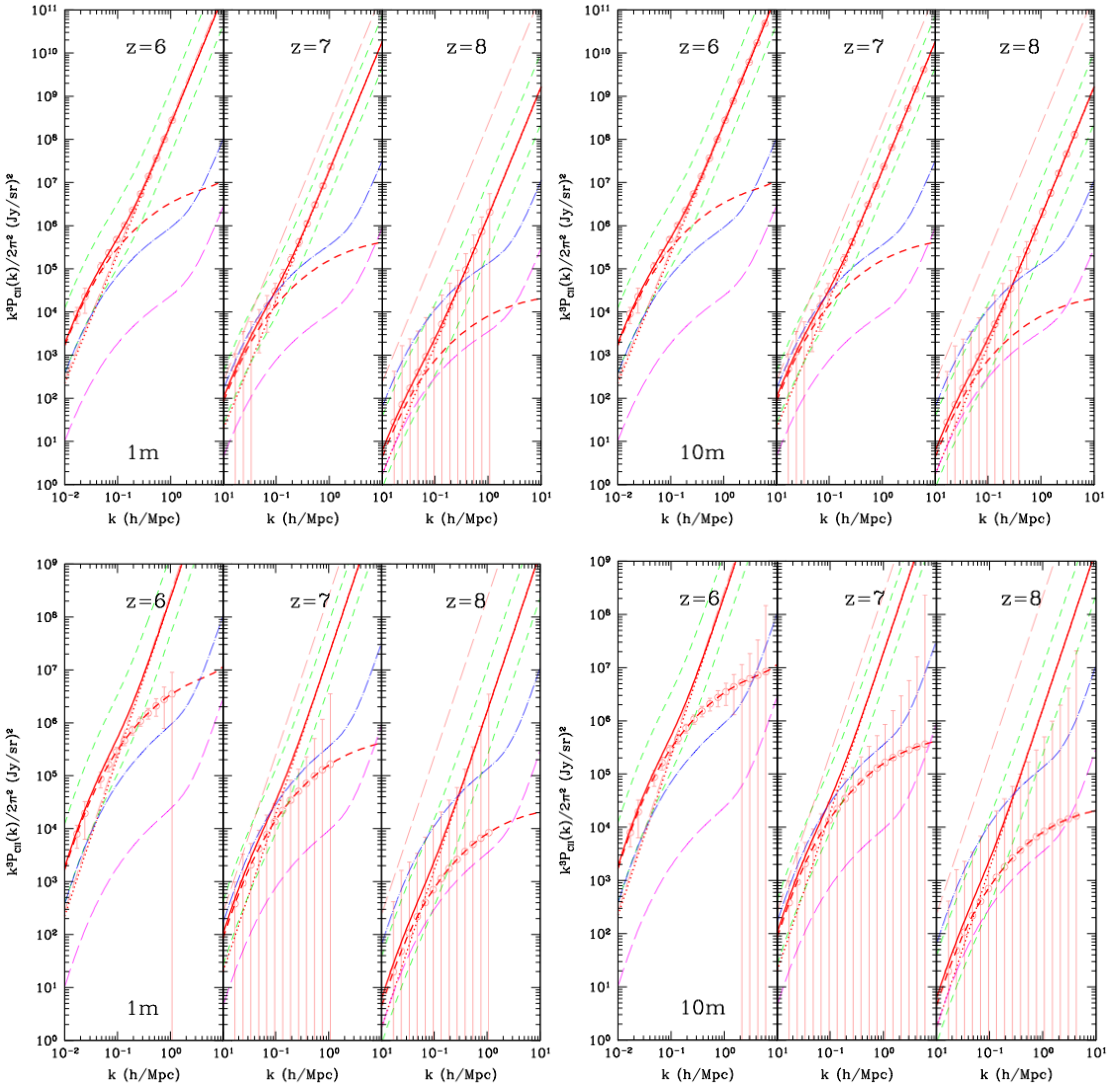

Figure 5.9: The clustering, shot-noise and total power spectrum of [C II] emission line at $z = 6$, 7 and 8. The red solid, dashed and dotted lines denote the [C II] total, clustering and shot-noise power spectrum respectively. The [C II] clustering power spectrum is estimated from a numerical simulation while the green dashed lines are the 68% confidence uncertainties in the [C II] power spectrum. The error bars and noise power spectrum (red long-dashed line) in the two panels are estimated with a 1 m aperture for [C II] line respectively. The magenta long dashed and blue dash-dotted lines are predictions on the [C II] power spectrum by scaling low-redshift observed relations such as the CO(1-0) to [C II] luminosity and a separate prediction in the literature by Visbal and Loeb (2011), respectively. Left plots refer to a 1-meter experiment, right to a 10-m. Top plots show errors on the total, lower plots show errors on the clustering signal.

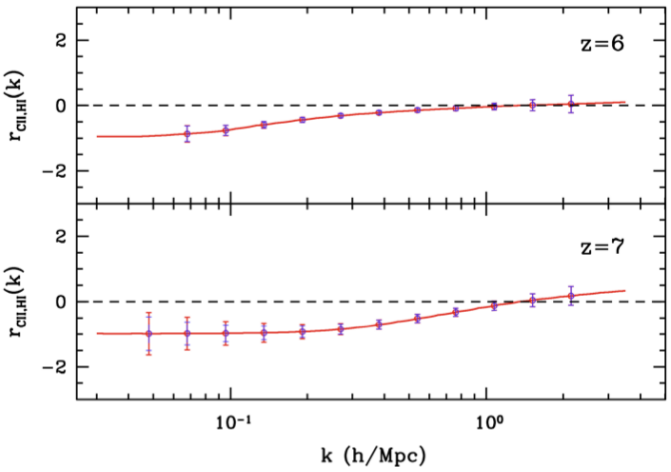

Figure 5.10: Cross correlation between [C II] and H I in the widefield experiment. There is an anti-correlation on large spatial scales. This anti-correlation decreases as reionization proceeds, and becomes slightly positive on small scales, reflecting the size scale of the individual ionized bubbles. The correlation of CO and H I should have a similar behavior.

source of ionizing UV photons is dominated by massive stars or stellar remnants, and may prove a more reliable tracer than CO or [C II] which rely on star formation and metal enrichment.

The Ly-α photons therefore trace a third phase of the ISM: ionized, recombining gas, and this probe therefore offers a complementary measure of galaxies and their environment—specifically, how many ionizing photons the stellar populations produce and how they are processed. However, unlike CO and [C II], these photons are strongly affected by their radiative transfer through the galaxy's ISM and the IGM around it. The Ly-α line is therefore most effective in comparison with other studies, either of broadband galaxy populations or other emission lines. For example, Schenker et al. (2012) find hints that the fraction of luminous galaxies with strong Ly-α emission declines suddenly at $z \sim 7$. In fact, Ly-α emission from individual galaxies is one of the most popular probes of reionization. However, it is very difficult to interpret these observations because the signal from a given galaxy depends on its complex internal physics. On the other hand, intensity mapping is less subject to these uncertainties because it also captures photons that scatter outside of galaxies, at least in principle.

While there are several predictions of the Ly-α signal for intensity mapping (also often known as tomography in this part of the literature), they have not been revisited in light of modern reionization models (like the CO and [C II] signals have been) and in the context of multiple probes of reionization (and cross-correlations between them). More theoretical effort is certainly needed to build robust models of the diffuse emission and the physical parameters that can be extracted from these data.

However, some work has recently been done to understand the emission around individual unusual objects. Cantalupo et al. (2008) investigated the brightness of Ly-α emission from quasar ionization fronts during reionization, and concluded that collisional excitation in partially ionized gas at the boundaries of bubbles (see Figure 5.11) was significant. They predict a line surface brightness of $\sim 10^{-21}$ erg s^{-1} cm^{-2} Å^{-1} arcsec^{-2}, with line widths of 100–200 km s^{-1}. The brightness is roughly 10^{-3} of the zodiacal sky brightness in a $\lambda/\Delta\lambda \sim 1000$ spectral band, a level likely detectable in an optimized experiment.

Experimentally, Ly-α emission is redshifted into the near-infrared, 0.85–1.34 μm for redshifts $z = 7$–

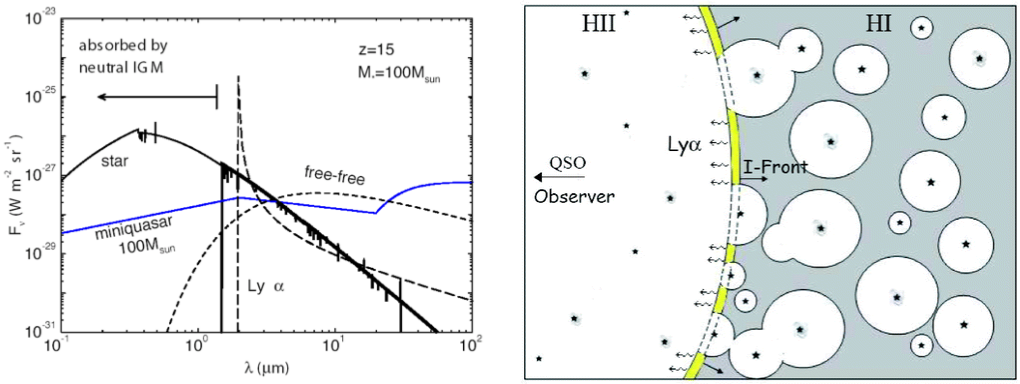

Figure 5.11: (Left) The emission spectrum of a 100 solar-mass star at $z = 15$. In addition to the stellar spectrum (solid line), we also show the nebular Ly-α (long dashed lines) and free-free (short dashed lines) emission of the ionized H II region surrounding the star, where the UV end of the stellar-spectrum (thin solid line) ionizes the surrounding medium. We assume that the nebula absorbs all ionizing photons. For comparison, we also show the flux spectrum associated with a 100 solar-mass black hole in the form of a mini-quasar. (Right) Schematic cartoon of neutral and ionized regions during reionization from Cantalupo et al. (2008). Ionizing photons from a bright quasar create an ionization front between the ionized and neutral regions, producing Ly-α photons from collisional excitation (yellow regions). Regions that are already ionized appear as holes in the Ly-α map at a given observed wavelength.

10. While searches for Ly-α background intensity or its anisotropies is still lacking in the literature, the astronomical community has focused on individual detections of bright Ly-α emitters through narrow band imaging surveys in 8–10 m telescopes (e.g., Stark et al. 2007, 2010). Successful studies at $z \sim 6$ show that Ly-α emitters are likely small galaxies with star-formation concentrated on 1 kpc sizes with star-formation rates less than 10 solar masses per year. The suggested space density of the brightest of these galaxies at 10^{-4} Mpc^{-3} (e.g., Pirzkal et al. 2007; Ono et al. 2012; Ouchi et al. 2010) converts to typical bias factors for the clustering of these galaxies of order 4 to 6. These initial observations suggest that Ly-α background is strongly clustered, while at the same time allowing a probe of small galaxies present during reionization that will remain undetected in targeted searchers (Y. Gong et al., in preparation).

Searches for the near-infrared extragalactic background (and Ly-α emission in the EBL) by absolute photometry have been problematic at these wavelengths due to the removal of foregrounds, chiefly zodiacal light, i.e., scattered sunlight from interplanetary dust grains in our solar system. New experiments may improve on this situation by either monitoring zodiacal light using the intensity of Fraunhofer lines (Bock et al. 2006; Kutyrev et al. 2008), or by conducting measurements outside the majority of the interplanetary dust cloud by going to larger radial distances or out of the ecliptic plane. However the field has also been developing experiments to probe the near-infrared EBL based on spatial fluctuations. These experiments are possible due to the spatial smoothness of the zodiacal light (Abraham et al. 1997; Kashlinsky et al. 2005; Matsumoto et al. 2011). Furthermore since our view through the interplanetary dust cloud changes around the Earth's orbit, measurements can exclude a zodiacal origin by observing the same region of sky at different times of the year.

Given the limited theoretical work on Ly-α tomography to date, the theory for EBL fluctuations may be informative. Current fluctuations measurements use multiple broad spectral bands with a wide field of view to search for an EBL component associated with reionization. A Ly-α tomography experiment would similarly measure spatial fluctuations in a series of $\lambda/\Delta\lambda \sim 1000$ spectral bands; continuum emission from

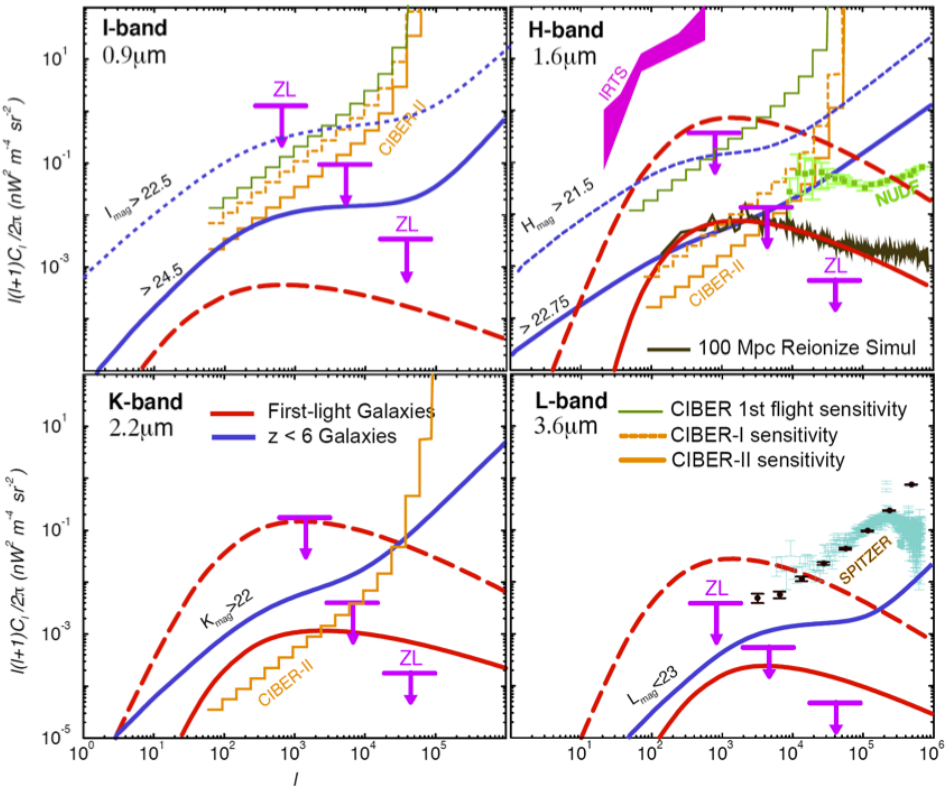

Figure 5.12: Spatial power spectrum of EBL fluctuations in selected IR bands. The red curves show the power spectra of fluctuations from first-light galaxies forming over the redshift interval $8 < z < 15$. The top red dashed line shows the case where fluctuations are normalized to *Spitzer* IRAC measurements. The bottom solid line shows the minimal signal necessary to produce reionization. Fluctuation measurements are shown for *Spitzer* IRAC and *HST* NICMOS in deep, narrow fields. Cyan points show *Spitzer* measurements by Kashlinsky et al. (2005) while black points show residuals from Cooray et al. (2004) after subtracting faint, blue dwarfs detected in deep HST ACS images. The dark blue curves give estimated fluctuations from known galaxies, as a function of magnitude cutoff, based on a galaxy distribution model matched to existing clustering data. The galaxy fluctuation signal is a combination of clustering, dominant on large scales, and shot noise, increasing as ℓ^2 and dominant on small scales. The galaxy cutoff taken for CIBER is 25% pixel removal using deep ancillary source catalogs. CIBER-II (solid blue) has a lower residual local galaxy foreground due to its smaller pixel size compared with CIBER-I (dashed blue). The orange stairsteps in three panels shows the $\Delta\ell/\ell$-binned statistical sensitivity of CIBER-I (in 2 bands) and CIBER-II (in 4 bands) instruments in a single 50s observation. The thin line shows the statistical sensitivity achieved in the first flight in February 2009, while statistical sensitivity in the second flight in July 2010 are close to the design goals. Zodiacal light is known to be spatially uniform, shown by the upper limits based on *Spitzer* and *Akari* scaled from mid-IR wavelengths. The black line shows the EBL fluctuations resulting from a 2048^3 particle, large volume (100 Mpc) numerical simulation of reionization with a combination of both Pop II and Pop III stars in first-light galaxies. The shape of fluctuations is model independent and shows the overall bump at $\ell \sim 1000$ in agreement with the analytical model.

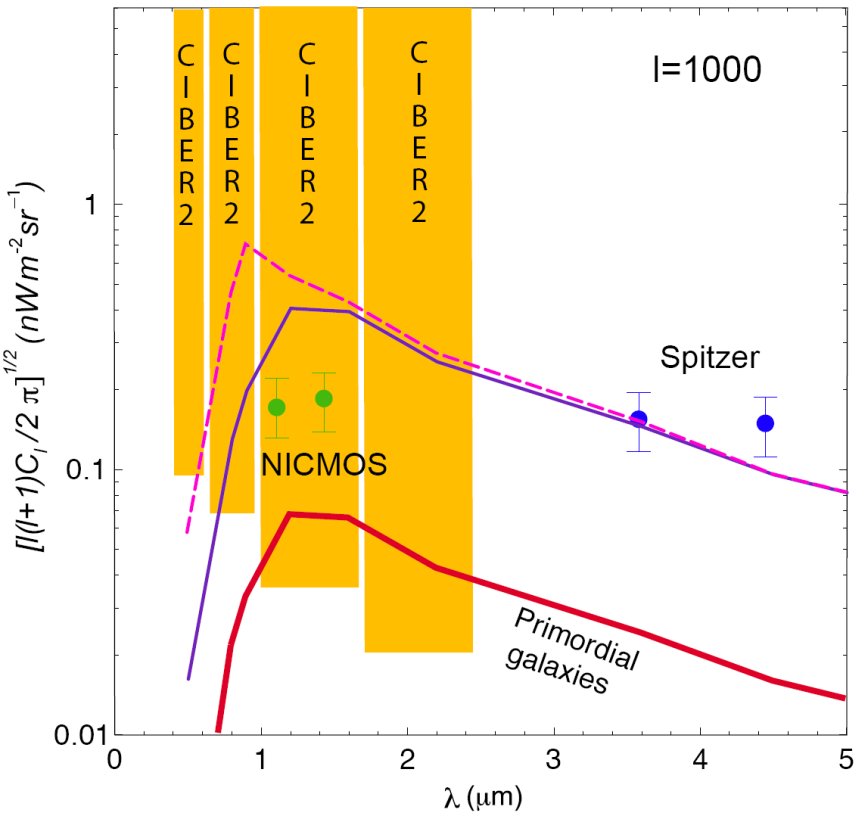

Figure 5.13: The relative sensitivities to first-light fluctuations are shown for CIBER-II at an angular scale of $10'$. Also shown are the rms fluctuations measured by *Spitzer* and *HST* NICMOS, extrapolated for comparison to the same spatial scale for reference. The modeled electromagnetic spectrum of first-light galaxy fluctuations in the top two lines, based ociber2n the model described in text for slow and fast reionization histories, is normalized to the *Spitzer* detection at 3.6 μm. The lower thick red line is the minimum expected from reionization. CIBER-II can probe down to the minimum reionization model in a short 50 s integration.

stars and free-free emission likely dominate over Ly-α emission in a broad-band measurement. Predicted spatial power spectra are shown in multiple spectral bands in Figure 5.12. The theoretical curves (adapted from Cooray et al. 2004) represent the clustering signal from reionizing galaxies for two cases. The higher curve is empirically fit to reports of EBL fluctuations with *Spitzer* (Kashlinsky et al. 2005) and extended to short wavelengths based on a spectral shape for reionization. The lower curve is based on a reionization model that produces the minimum photon background to initiate and sustain reionization. The electromagnetic spectrum of the reionization-EBL is shown in Figure 5.13, peaking at a wavelength of $\sim$ 1.5 μm due to the continuum spectrum with the Ly-cutoff, with a contribution from Ly-α line emission.

Interestingly, fluctuations from the reionization EBL are easily detected, as shown in the statistical sensitivity in just a 50 s integration for the current CIBER1 sounding rocket experiment and the CIBER2 planned follow-on with a 30 cm telescope. Clustering and Poisson fluctuations from local galaxies present a significant astrophysical foreground. Experiments must have fine enough angular resolution ($\sim 5'$) to mask these galaxies based on a catalog of sources from large-area galaxy surveys.

Finally, Ly-α surveys are being developed to trace out recombination line emission associated with

the cosmic web. The Keck Cosmic Web Imager (KCWI; Martin et al. 2010) uses an integral field unit covering wavelengths 0.35–1.05 μm, with selectable resolution $\lambda/\Delta\lambda = 1000$–20,000 and field of view $20' \times (7\text{–}30)'$. The Cosmic Web Imager (CWI; Matuszewski et al. 2010) is a spectrometer for the Hale 5-m telescope that is similar to KCWI, with spectral coverage 0.38–0.95 μm, resolution 5000, and field of view $60' \times 40'$. These instruments will excel in measuring Ly-α emission from compact objects, and may be able to map filamentary structures in the cosmic web at lower redshifts (Furlanetto et al. 2003). However, as noted by Martin et al. (2010), tracing out emission from reionization, and measuring faint bubble features over many-arcminute scales, will be extremely challenging given the small fields of view and atmospheric airglow emission at the longer wavelengths needed for $z > 6$.

Ly-α is potentially a powerful line tracer of the epoch of reionization, but further theoretical work is needed to determine the spatial and redshift structure from a line survey, and to quantify the possible range in surface brightness. In addition, foreground confusion from low-redshift galaxies must be determined. A specialized wide-field high-throughput near-infrared spectrometer needs to be developed to tomographically map Ly-α emission from reionization. Experimentally it may be challenging to carry out this survey from the ground owing to airglow emission, but this scenario should be investigated, perhaps confined to imaging in limited bands between the OH airglow lines. A small-aperture space-borne telescope may be able to carry out such a survey, mapping the large areas of sky appropriate for comparison with 21-cm surveys, with high sensitivity in a low-background space environment. A modest study is needed to develop the theoretical case in conjunction with ansatz experiments, allowing us to compare with the scientific potential with CO and C^+ line surveys.

In addition to the Ly-α emission, the optical and UV continuum radiation from first light is present today in the near-infrared extragalactic background light (EBL). Searches for this radiation based on absolute photometry have proven problematic due to confusion with the Zodiacal foreground. However, a first-light component must exist in the near-infrared EBL, based on a lower limit to supply enough photons to ionize the IGM. Such "minimal" reionization scenarios produce an EBL ~ 1 nW m^{-2} sr^{-1} (Chary & Cooray 2010), a level undetectable by current absolute photometry measurements which, after dedicated space-borne measurements, show large discrepancies. Nevertheless, in principal, near-IR fluctuation maps could be cross-correlated them other probes of reionization, including H I 21 cm maps. Theoretical studies that model both stellar emission and gas physics are needed to understand the astrophysical information that can be probed with such a measurement.

We note that near-IR fluctuations, including Ly-α, and CO tomography together would probe both the star formation rate (from CO) and the stellar mass (from near-IR), the combination of which provides overall star formation efficiency in the early Universe.

5.4 Additional Redshifted mid- and far-IR transitions from space

As the example galaxy spectrum in Figure 5.14 shows, [C II] is only one of several spectral transitions which each carry luminosity of order 10^{-3} times the galaxy total. Fine-structure transitions of ionized silicon [Si II] and iron [Fe II], doubly- and triply-ionized oxygen [O III], [O IV], and a series of ionization states in neon [Ne II], [Ne III], [Ne IV], [Ne V] with wavelengths ranging from 12 to 88 μm are also very bright. Ratios among these transitions are set by the ionizing UV field strength and hardness (color temperature), as well as metallicity. They therefore can provide information about the stellar mass function and the presence of black-hole accretion systems and may offer a way to probe the evolution of the ionizing sources with cosmic time through the reionization epoch.

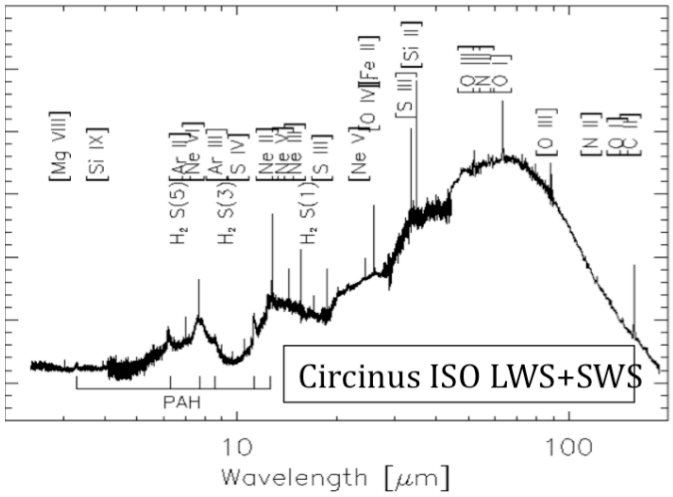

Figure 5.14: Complete mid- and far-IR spectrum of a nearby galaxy obtained with the long-wavelength spectrometer (LWS) on the *Infrared Space Observatory* (ISO). [C II] is one of a handful of powerful fine-structure, H_2, and PAH transitions.

In addition to the fine-structure transitions, the quadrupole rotational transitions of H_2, and the powerful polycyclic aromatic hydrocarbon (PAH) emission features from small dust grains lie in this rest-frame mid-IR band. These two probes are complementary: H_2 probes the molecular material regardless of its enrichment, and is the primary cooling pathway for pristine metal-free gas. The PAH features (at 6.2, 7.7, 8.6, 11.3, 12.7, and 17 μm) are broad ($dl/l \sim 10$) so they carry 5–10 times the power of even the brightest gas-phase lines, and do not suffer from optical depth effects. They may therefore be among the most readily detectable indicators of heavy-elements in the early universe.

For this band with rest-frame wavelength shortward of [C II] the epoch of reionization is inaccessible from the ground; the atmospheric is essentially opaque from 20 to 300 μm. However, for wavelengths between 2 μm and 3 mm, a cryogenic space telescope offers a substantial advantage in sensitivity over a comparable ground-based system. While the ground-based telescope is limited by the thermal emission of the telescope and atmosphere, a cold system in space can be limited only by the solar-system and galactic dust emission. This advantage is particularly appropriate because the reionization epoch experiments we are considering do not require large apertures, but do require optimal surface-brightness sensitivity. Figure 5.15 shows this sensitivity advantage as calculated for the proposed 3.2-m SPICA telescope[2] and JPL's proposed BLISS spectrometer (Bradford et al. 2010). In terms of sensitivity to mean intensity in energy units (again independent of angular resolution), the space system can be (conservatively) a factor of ~ 20 more sensitive than the [C II] experiment we outlined above. Thus, an experiment with the same format but designed for a cold space system could measure the [C II] intensity (or that of comparably-luminous transitions) at least 400 times faster than the ground-based system.

BLISS, as currently configured, is optimized for point-by point studies of pre-selected galaxies; it has two simultaneous beams on the sky covering the full 38–430 μm range. It is thus not optimal for the blind mapping of the reionization tomography experiments. However, the raw sensitivity advantage means that even the 2-beam BLISS/SPICA may be able to measure line intensity measurements over small fields

[2] http://www.ir.isas.jaxa.jp/SPICA/SPICA_HP/index_English.html

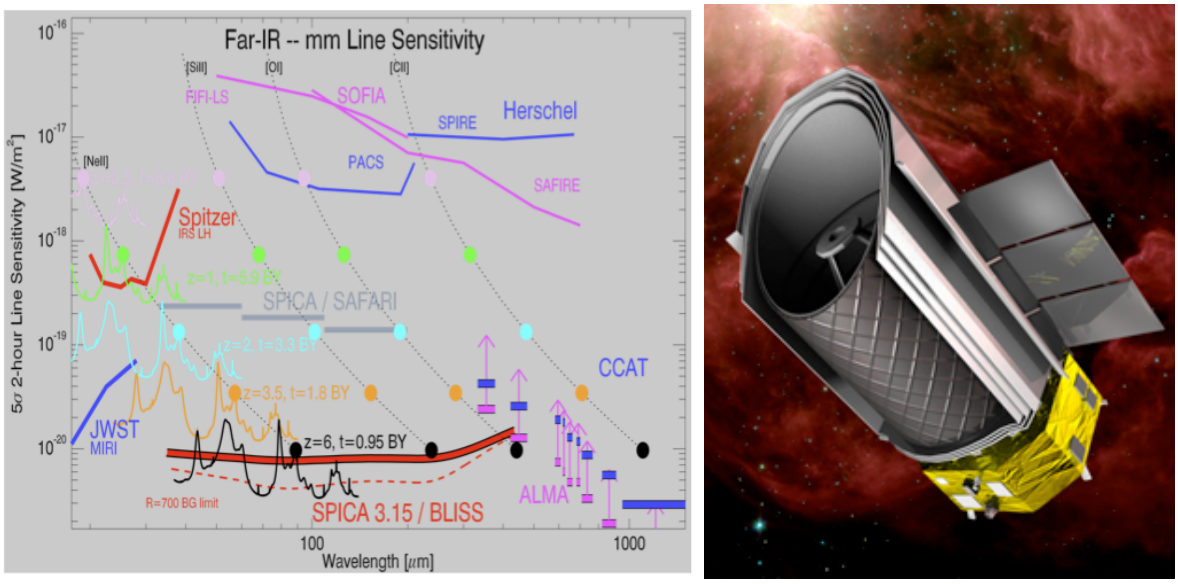

Figure 5.15: Sensitivity of a cold space telescope such as the proposed SPICA mission. SPICA is a Japanese-led 3.2-meter telescope actively cooled to below 6 K and deployed to the earth-sun L2 which could fly as early as 2020. BLISS is a proposed JPL-build spectrograph optimized for wide-band point-source spectroscopy. The cold space platform can be at least 20 times more sensitive than any ambient-temperature telescope in $\mathrm{W\,m^{-2}\,sr^{-1}}$, and thus several hundred times faster for a given line measurement. Plotted sensitivities are for measurement of point sources; they include the telescope area which improves the sensitivity of CCAT and ALMA relative to the ∼3-meter class space missions. This factor is not applicable to a reionization tomography experiment.

using the [Ne II] or [Si II] transitions. Regardless, a dedicated wide-field cryogenic experiement will likely be a strong candidate for a future mission to probe the epoch of reionization, especially given that the required aperture $\sim$ 1 m or less at these wavelengths.

6

Required technical development

In this section we discuss the instruments required to measure the spectroscopic signals from the early Universe described in Sections 4 and 5. Both ground-based and space-based platforms will be needed to fully study the cosmological signals, and technical developments will be needed in several areas. The Study concluded that technical work is most urgent for the CO and [C II] intensity mapping programs, and we present roadmaps for these. The technical development for CO mapping will also be useful for the even more difficult recombination line studies.

6.1 Instrument requirements and challenges for studies of recombination lines

For the recombination-line all-sky (monopole) spectral measurement, where the relative spectral resolution is 10% (e.g., 1 GHz resolution at a frequency of 10 GHz) and the system temperature is 20 K, reaching a thermal sensitivity limit of 10 nK requires averaging over ~ 1000 independent feeds for 1000 h, according to the radiometer equation. This is a large number of feeds to accommodate, and requires new technical development to do affordably, particularly since a space-based platform is almost certainly necessary for the measurement in order to escape atmospheric fluctuations.

The largest hurdle, however, to the desired measurement is calibrating the instrument. Since the Galactic foreground emission is only ~ 1 mK at 10 GHz, the spectral dynamic range required is set by the CMB blackbody emission and is roughly $2.7\,\mathrm{K}/10\,\mathrm{nK} \approx 10^8$. Unlike FIRAS, which characterized the absolute blackbody spectrum of the CMB, the strategy needed to detect and characterize recombination-line features can abandon the conventional absolute calibration requirement of a radiometer in favor of a differential spectral calibration requirement. It is exceedingly difficult to conceive of any radio instrument that could make an absolute measurement at 1 part in 10^8—in any environment—whereas high-precision differential measurements are routinely achieved by radio instruments on the ground and in space. An excellent example is *WMAP*. The differential radiometers on *WMAP* have achieved dynamic range of $> 10^6$.

The distinction between a recombination line experiment and *WMAP*, however, is that the line measurement is a differential spectral measurement rather than a differential angular measurement. Radio antennas and receivers have properties that are dependent on frequency. The beam pattern of the antenna changes with frequency, the impedance of the antenna, waveguide, and electronics, and the internal noise contributions all change with frequency. Furthermore, the best calibrator sources produced today (e.g., Figure 6.1) are known only at the level of 1 part in 10^6, at best.

The challenges, therefore, that must be addressed to enable sensitive recombination line all-sky measurements are to develop:

- An array of light-weight, low-cost, broadband feeds with carefully controlled frequency-dependence;
- High-bandwidth spectral correlators;
- Calibration sources and strategies capable of reliably (and provably) achieving a relative spectral dynamic range of 1 part in 10^8 or better.

The primary calibration issues that must be addressed include:

- Galaxy power varies across spectrum, which leads to frequency dependent systematics;
- Galaxy and CMB power varies with angle, which can be coupled into the spectral measurement through frequency-dependent sidelobes, and cause time-dependent systematics;
- Reflections between calibrator and feeds are difficult to model or measure;
- Any residual polarization in the calibrator will corrupt the intensity calibration.

We note that missions to measure CMB spectral distortions have been proposed in the past, including FIRAS II and the Primordial Inflation Explorer (PIXIE), but these concepts were not targeting recombination lines.

6.2 Instrumentation for CO intensity mapping

The key technical drivers which arise from the science requirements for CVO intensity mapping are: The need to explore a decade of spatial-frequency scales $k = 0.1$–$1.0\,\mathrm{Mpc}^{-1}$ (corresponding to approximately 1 deg to 6 arcmin); and the need for approximately 1000 receiver elements in order to achieve the required sensitivity in a reasonable timescale. In addition, we wish to study both the CO(1–0) and the CO(2–1) transitions (which, for the redshifts of interest, are centered at frequencies around 15 and 30 GHz respectively) and we assume that these will likely require separate, scaled telescopes. Two experimental approaches to achieve these goals were identified, a Focal Plane Array (FPA) on a single large dish and an interferometer. Both of these approaches should be studied to identify their individual technical and cost implications, as well as issues which both approaches have in common. Key challenges were quickly identified for the two approaches: for the FPA approach, whether it is feasible to pack 1000 detectors with sufficiently accurate beams into the focal plane of a telescope, which at the same time is not prohibitively expensive to manufacture (especially for the 20 m dish size needed for 15 GHz); for the interferometer, whether the required correlator would be too expensive and consume too much power during operation. Plausible solutions were identified for both of these challenges and further investigation will be required to prove them viable and to identify the optimum approach. We now discuss these and other issues in greater depth and outline a roadmap which leads through a prototyping stage to construction of the science grade instrument.

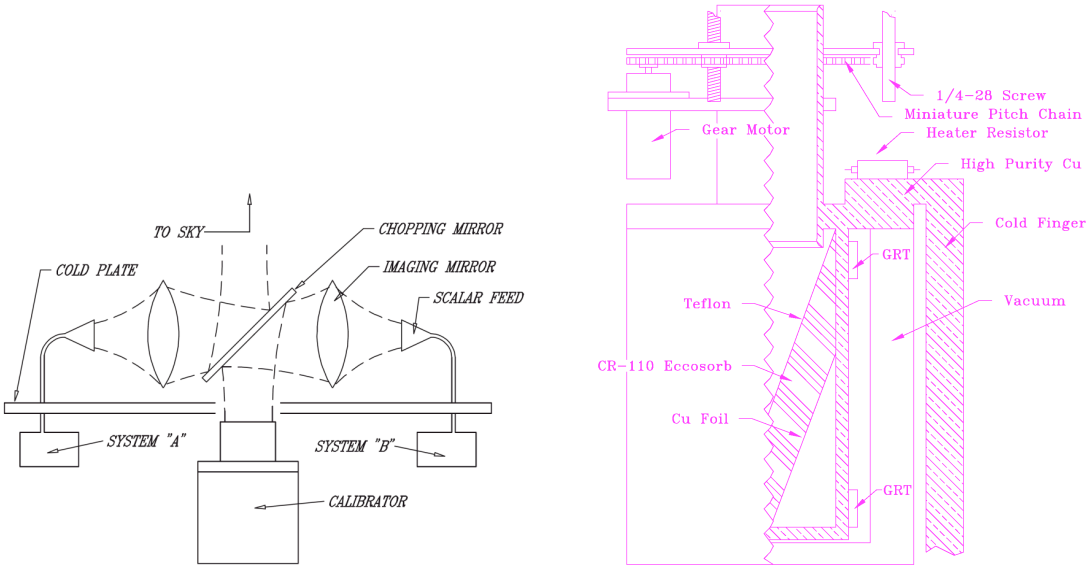

Figure 6.1: Example of a high precision microwave calibrator design from the Ph.D. thesis of Schuster (UCSB).

6.2.1 Approach 1: Multi-feed interferometer

The instrument requirement can be represented as a filled aperture of a given size D (chosen to give the correct resolution), with a number N of receivers (to give sufficient sensitivity). One way of implementing this is with a single aperture antenna fed by a focal plane array with N elements. An equivalent implementation is to take the same sized aperture and break it up in to N smaller antennas, each with a single feed, and then correlate the outputs of all the feeds. This arrangement has the same sensitivity and field of view as a single dish with a focal plane array, but has several advantages. The correlated baselines have no sensitivity to total power, and so atmospheric fluctuations and receiver gain stability fluctuations are removed from the data. Individual antenna feed signals can be phase-switched, and the baseline signals synchronously detected at these switching frequencies, further rejecting instabilities in the electronics. However, the number of baselines that must be correlated is $N(N-1)/2$, which can be very large. For example, if $N = 1000$ and the correlated bandwidth is 10 GHz (and hence the sample rate is 20 GS/s), the rate of multiply-accumulate (MAC) operations required is 4 (per complex multiply) $\times 1000 \times 999/2 \times 2 \times 10^{10} = 4 \times 10^{16}$ MAC/s. In current technology this would need about 50,000 large FPGAs to implement, at a cost of many tens of millions of dollars. This calculation is for the cross-correlation part of an FX architecture, which is expected to dominate the computational requirements. In addition, a spectrometer element per feed is required, but this is common to all implementations, including a focal plane array. The approximate total performance required for the spectrometer is $8\log_2(N_{\rm chan})\times$ sample rate per element, i.e., 1.6×10^{11} MAC/s per element or 1.6×10^{14} MAC/s in total for 1024 channels across a 10 GHz band.

The same performance can be achieved at much lower cost by effectively aggregating antennas in to larger individual antennas, and recovering the field of view per antenna by equipping each with multiple feeds. If the number of antennas is reduced by a factor M, and each is equipped with M feeds, then the size of correlator required is reduced by a factor M^2 per feed, but M separate correlators are required to correlate the corresponding feed of each antenna. Each feed/correlator images a field of view M times smaller than before, but across all the feeds the total field of view is unchanged, and overall the size of the

correlator required is reduced by a factor M. The signal for an individual feed is averaged over a larger area in the fourier plane, reducing l-space resolution, but this information can be recovered from the multiple pointing information from the multiple feeds.

To give some concrete numbers, suppose that the required resolution fixes the maximum baseline at 20 m, and $N = 1000$. For the full interferometer each of the 1000 antennas would have a diameter of 0.63 m, and have a single feed. If instead each antenna is equipped with a 19-feed cluster, the area of each antenna is increased by a factor 19, so the diameter is $0.6\sqrt{19} = 2.75$ m. Fifty such antennas give the total collecting area, and each of the 19 parallel correlators has to deal with 1,225 baselines.

The number of antennas has, however, to be kept high enough that the Fourier plane is well sampled, giving high-quality imaging with no gaps in the *uv* coverage. The number of independent patches in the *uv* plane (i.e., the number of points required to Nyquist sample the aperture) is roughly $(2D_{\rm max}/D_{\rm dish})2$, or in the case of a fully-filled aperture, $4N_{\rm dish}$. In the above example this is 200, so the number of visibilities exceeds the number of independent patches by a factor of ~ 5 (but they are not uniformly distributed). Increasing the dish size (and number of feeds per dish) further may therefore be possible until the aperture plane is no longer fully sampled.

If a larger spatial dynamic range is required, then multiple antenna sizes (with more feeds on the larger antennas) can be used.

The above argument assumes that the interferometer antennas can be closely packed, and this requires that they be co-mounted—individually tracking antennas with high filling factor will have very limited tracking range due to shadowing, which will restrict the integration time per field that can be achieved. Ideally such a co-mounted array would also have a boresight rotation axis (e.g., as on CBI) which allows control of parallactic angle, and modulation of parallactic angle can be used to control ground radiation effects. In order to maintain the high filling factor, on-axis antennas are preferred. There are however several potential problems with this that need addressing. To minimize scattering to large angles, solid secondary support legs are to be avoided—the secondary can be supported on transparent dielectric (feasible for small antennas). Direct reflection paths back to the feed which result in standing waves and hence frequency-dependent gain variations must also be avoided. An optical design must also be found which allows multiple feeds on a fairly small antenna without excessive secondary blockage.

Cryogenics are often an expensive component in capital and operations costs—and a large-N interferometer has to maintain many such units. As in most systems, going colder is better; however coolers to about 60 K are cheap and reliable. Trade-off studies of, say, 60 K versus 20 K, will be instructive in terms of LNA performance since it is not necessarily the performance-limiting factor. As these structures are intended to be densely-packed, sharing of infrastructure is possible. Certainly compressors can be shared and an investigation of multiple cold-heads per cooler and/or pumping cryogenic fluid may be important, particularly if 20 K is needed (as expected).

DACOTA

A subset of the workshop explored in depth the interferometer concept for CO intensity mapping. The proposed instrument, the Dense Array for Cosmological Transitions (DACOTA), employs a phased approach to characterization and detection of the cosmological signal. The design emphasizes coherent integration on a subset of baselines to maximize sensitivity to the angular power spectrum. An array of densely packed antennas on a single platform avoids problems with shadowing for the closely-spaced antennas. Third axis rotation of the platform with respect to parallactic angle enables the baseline orientations to remain fixed

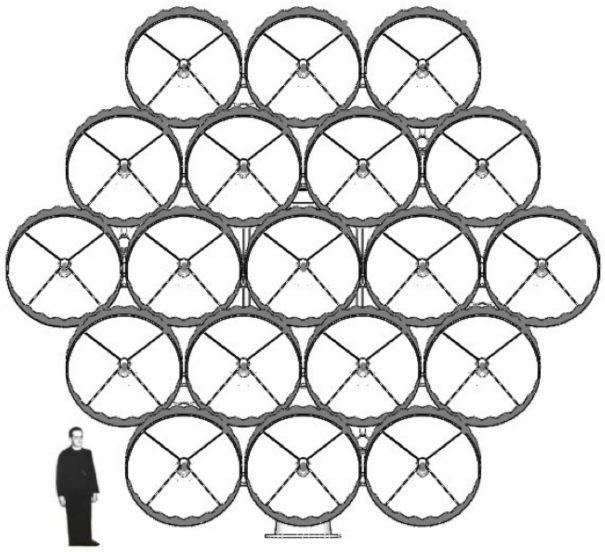

Figure 6.2: Artist's impression of a 19-element co-mounted inteferometer array for DACOTA.

with respect to the source as it moves across the sky. Figure 6.2 shows an image of a 19-element DACOTA platform. Higher sensitivity can be achieved through increasing the number of platforms and/or the number of elements per platform.

Traditionally, power spectra have been obtained only from two-dimensional angular measurements on the sky. DACOTA can exploit the full three dimensional angular power spectrum, which is obtained from frequency-dependent visibilities as follows:

$$P(k > k_{\rm min}) \propto V^2(u, v, \eta) \,,$$

where P is the angular power spectrum, V is the visibility, u, v are the standard orthogonal baseline coordinates and η is the Fourier component conjugate to the frequency axis. The interferometer can be configured to optimize its response to many coherent repeated measurements of a small number of baselines to gain sensitivity to enable detection. Writing the sensitivity for this, we can show its dependency on telescope design/performance parameters:

$$\Delta^2_N(k) \propto \frac{{T'_{\rm sys}}^2}{D^2 N^{1.1} \tau \sqrt{\Delta\nu}}$$

where $T'_{\rm sys}$ is the system temperature over the efficiency, D is the antenna diameter, N is the number of antennas (and receivers), τ is the integration time, and $\Delta\nu$ is the total bandwidth. $N^{1.1}$ is a power-law fit to baseline distributions and holds for N from 7 to 273 for k values near $k_{\rm min}$. It is a steeper function at higher k values.

For redshifted CO at $z \sim 6$–7, the antenna diameter will be about 1 m to probe $k \sim 0.1\,{\rm Mpc}^{-1}$ and greater. To make up for the rather small diameter (which is advantageous for practical antenna construction and pointing reasons), we need to build many elements. Figure 6.3 shows the predicted sensitivity of a 3-axis 19-element platform of 1.2-m antennas for the CO(2–1) transition along with bracketing models

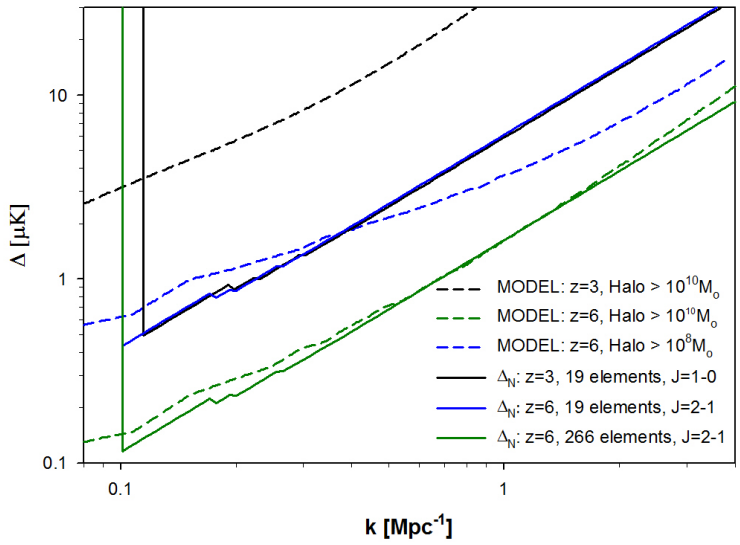

Figure 6.3: Expected sensitivity of DACOTA.

of the signal from Lidz et al. (2011). The bracketing values are models with a very large minimum halo mass ($> 10^{10}\,M_\odot$) and with a relatively small minimum halo mass ($> 10^{8}\,M_\odot$). Also shown is a larger array comprising 14 19-element platforms, as well as the signal and performance at a redshift of $z = 3$ for a single 19-element platform. The instrumental sensitivity assumes a single pointing center, a bandwidth of 2 GHz and 1000 h of integration.

Figure 6.3 indicates that realizable arrays may detect the signal for a plausible range of models. Systematics can be addressed through cross-correlation of the detected signal with a separate CO transition or with galaxy distributions from large area optical spectroscopic surveys. A stand-alone DACOTA experiment would consist of two arrays for detection of CO(1–0) and CO(2–1) transitions, with dishes and array spacings scaled by a factor of 2.

Many of the technology challenges for DACOTA are shared with the focal plane array approach, namely, affordable high-quality wide-bandwidth receivers and low-cost, low-power, high-bandwidth, and large-N correlators. The receivers are not as tightly integrated as for a large focal plane array, which chiefly impacts the cryogenic system, however an interferometer should naturally have lower systematics. Development of low-noise robust amplifiers that operate well at higher temperatures (60 K, for instance) would provide significant simplification of the cryogenic system. Hierarchical correlation in which baselines within a platform are correlated and intra-platform baselines are correlated as phased array beams from each platform can significantly reduce correlation costs without sacrificing sensitivity to the CO signal. The antenna structures themselves are quite small and readily manufactured and handled. The use of a large platform that rotates along a third axis allows long coherent integration on a small number of baselines.

6.2.2 Approach 2: Focal Plane Array

A single dish with a focal plane array of ~ 1000 feed elements could be an effective and affordable strategy for making CO intensity mapping observations. The motivation for a focal plane array approach consists of the following points:

- Simpler than an interferometer: fewer telescopes, less computation required;
- Very high sensitivity as aperture area is fully utilized;
- Spectrometer design is relatively simple as each receiver is independent;
- Sensitivity scaling is $N^{1/2}$ where N is the number of horns;
- General purpose "machine"—can be easily reconfigured for future experiments;
- Beam size (FWHM) at 15 GHz given by $\theta = 100/D$ arcmin, hence only a single 10–20 meter dish is sufficient;
- Excellent sidelobe performance with high optical efficiency;
- Excellent rejection of non FOV point sources and galaxy and CMB;
- Very low ground pickup possible, leading to low $T_{\rm sys}$;
- Large focal planes possible;
- 100 horns at 15 GHz or 400 horns at 30 GHz are possible on a 10 m reflector (Figure 6.4);
- Both active scanning, drift scanning and active chopping strategies are possible;
- Single dish allows for flexibility in receiver—ability to mix focal plane;
- Multi spectral capability intrinsic to design;
- While a custom telescope may be needed we may be able to get time on an existing one to start testing;
- Pointing is easier as there is just one antenna to point —this is important as sidelobes are not varying as much.

The properties of a single dish with focal plane array for CO(2–1) and CO(1–0) line transitions are summarized in Table 6.1.

The costing model of antennas as a function of diameter and frequency has been looked at in a number of studies for the SKA and DSN (D'Addario 2008; Bunton 2007; DeBoer 2006; Weinreb 2006). Simplistically, the diameter and maximum frequency scaling are usually modeled as power laws. For diameter, the canonical value is $D^{2.7}$ while a range in $\nu_{\rm max}$ is quoted, however a good fit seems to be $\sqrt{\nu_{\rm max}}$. In addition, there are significant fixed costs for NRE and infrastructure, particularly for the first antenna. However there are currently a number of antenna designs that may be either directly usable or with minimal redesign to reduce the NRE costs. In some cases there may be existing antennas that could be used.

Based on estimates from existing facilities and from Bunton, for a mass-produced 20 m dish at 15 GHz, the cost will be $\sim$\$1.3M and a 10 m at 30 GHz will be $\sim$\$500k. Not included are the associated NRE costs, as well as the first unit premium for tooling, etc. Also not included are electronics or foundation or site infrastructure. Depending on the details, the full cost could be a factor of 2–4 greater.

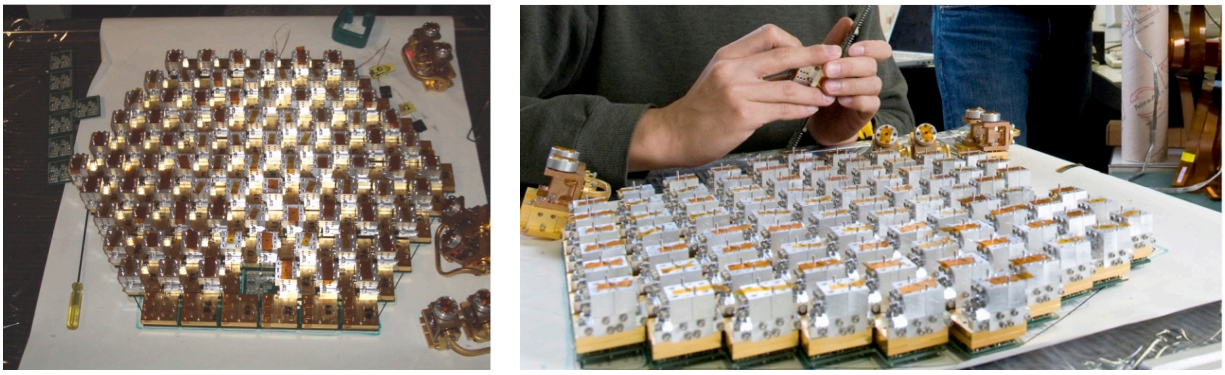

Figure 6.4: The QUIET 90 GHz focal plane array demonstrates the underlying technology of approximately 100 packaged miniaturized microwave receivers. This is significant faction of the $\sim$ 1000 elements needed for the proposed CO mapping instrument if implemented as a focal plan array on a single dish. Additional information on QUIET instrumentation is available at `http://quiet.uchicago.edu`.

Table 6.1: Properties of single dish focal plane array reference design

	14.4 GHz ($\lambda \sim 2$ cm)	28.8 GHz ($\lambda \sim 1$ cm)
Line	CO (J=1–0)	CO (J=2–1)
Rest frame frequency	115 GHz	230 GHz
Target redshift range	7–10	7–10
Frequency range	10.5–14.4 GHz	21.0–28.8 GHz
Antenna type	Reflector	Reflector
Diameter, D	20 m	10 m
Angular resolution	3.5–5.0 arcmin	3.5–5.0 arcmin
Bandwidth, B	$\sim$ 5 GHz	$\sim$ 10 GHz
Spectral resolution	0.01 GHz	0.01 GHz
Number of spectral channels	500	1000
Number of feeds	1000	1000
Feed size	$\sim 5\lambda$	$\sim 5\lambda$
Focal plane area	100,000 cm^2 (10 m^2)	25,000 cm^2 (2.5 m^2)
$T_{\rm sys}$ per beam	< 30 K	< 30 K
Instantaneous sky area	3 deg^2	3 deg^2

6.2.3 Antenna Feeds

Feed horns for the CO survey can be of several types. Ideally one feed horn would cover the entire band of interest from 10–40 GHz but in practice this is neither easy to realize nor desirable for practical reasons. Such broadband feeds do exist but their performance is poor compared to smaller bandwidth corrugated (shaped or linear) and shaped smooth-wall horns. Some dual-band corrugated feeds have also been developed, and should be studied. As a baseline we assume we want two bands, 10–20 and 20–40 GHz. Even this 2:1 bandwidth represents a significant challenge, but 2:1 corrugated feeds with decent performance have been made in certain circumstances. Much better performance is typically achieved with a 50% bandwidth. This area requires more study to determine the best approach.

The production of either smooth wall or corrugated feeds can be done by direct machining in this frequency range. Although electroforming is always possible, it is generally much more expensive. Corrugated feeds can be made via either direct CNC lathing or via plates or rings. All work well and it is a matter of final design that will dictate the best approach. For a large focal plane, the curvature of the focal plane may favor individual horns but this will have to be modeled. Smooth wall single machining operation (drill with a custom boring tool) is simple but broadband performance is an issue.

Various materials for horn production are feasible including metals and plastics. Direct 3D printing via plastic or laser sintering of metal powder is also possible. We will have to explore the tradeoffs but we can assume a baseline of machined aluminum using either direct lathing or plate/ring design. The cryogenic performance of aluminum is satisfactory and it offers good thermal conductivity. All of these techniques lend themselves to mass production.

Circularly symmetric corrugated and smooth wall horns offer good polarization separation with corrugated horns typically having superior cross polarization rejection and lower VSWR as well as better side lobe performance. Using both polarization states would be helpful but does complicate the design. Ideally all Stokes parameters (I, Q, U, V) would be measured but it may not be necessary. Where it may be helpful is in discriminating between foregrounds and RFI from the cosmological signal.

6.2.4 Low Noise Amplifiers

The CO reference designs require a large number of low noise receivers from 10–26 GHz (Ku/K-band) and 26–40 GHz (Ka-band). Since the telescope costs drive the overall system costs, and the sensitivity is linearly dependent upon the system noise temperature, it is imperative that the system be designed for the lowest possible noise. The large number of feeds required and the desire to simultaneously detect two orthogonal polarizations, drives the design towards an integrated approach.

At frequencies 10–40 GHz, the best noise performance is obtained with InP High Electron Mobility Transistors (HEMTs) operating below 20 K. Radio astronomy projects including CBI-2, *Planck*, *Herschel*, EVLA and ALMA employ transistors from the TRW (now NGC) 100 nm InP process.

Ku/Ka Band: In the frequency range 10–26 GHz the best results have come from discrete transistors in custom tuned microwave integrated circuits (MICs). An example of the performance of one such amplifier produced for the EVLA is shown in Figure 6.5 and has noise of 8–10 K from 20–26 GHz. Similar performance can be obtained with monolithic microwave integrated circuit (MMIC) amplifiers with tunable input stages. An example of this is shown in Figure 6.6. There are no current designs which cover 10–26 GHz band in one or two channels. This means that amplifiers will need to be designed in either MIC or MMIC technology to minimize the number of receiver bands.

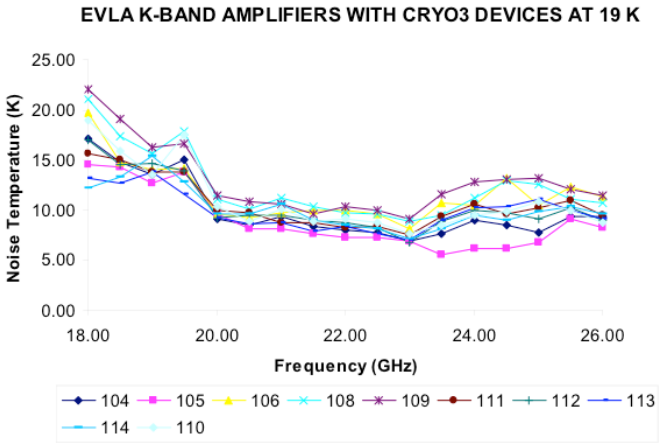

Figure 6.5: Noise temperature of EVLA amplifiers using 10 nm InP transistors (M. Pospieszalski, private communication).

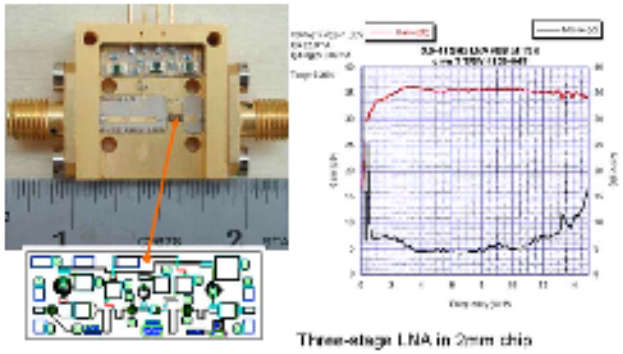

Figure 6.6: X/Ku band low noise amplifier with noise of 5–10 K over the frequency range 10–14 GHz.

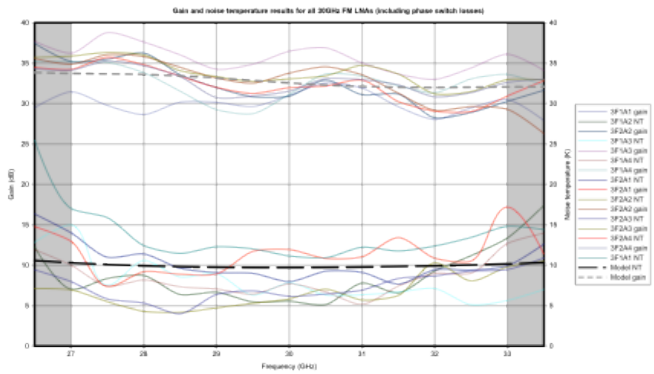

Figure 6.7: Planck-LFI front-end module noise performance.

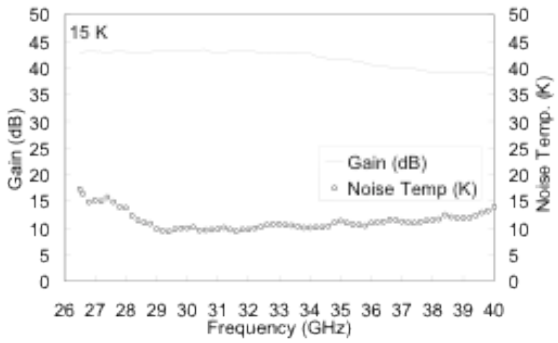

Figure 6.8: Noise performance of a MMIC low noise amplifier covering 26–40 GHz.

Ka-Band: At Ka-band, the best published results also arise from the TRW 100 nm InP process. The *Planck*-LFI receiver noise curves (based upon the NRAO EVLA design) are shown in Figure 6.7. The performance is 5–10 K for the low noise amplifiers. The on-orbit performance for the full receivers is closer to 10–11 K for all channels. Given the number of receivers needed, it is worth examining the performance of integrated approaches. MMIC amplifiers at Ka-band include a three-stage 100 nm InP device with 10–15 K noise (Figure 6.8). It is clear from this that if there is a noise penalty to be paid in going from MIC to MMIC, it is less than 3 K. While that is not a very large factor, it is worth exploring ways to improve the MMIC approach. Models have shown that employing the new generation of 35 nm transistors can improve the performance at Ka-band as much as a factor of two ($T_{\rm LNA} \sim 5$–7 K). Such improvements are less likely to be realized at lower frequencies as second order effects such as gate leakage are more likely to dominate the noise properties.

In order to facilitate integration of the instrument, it is highly desirable to integrate as much of the receiver as possible in a mass producible front-end. QUIET was able to integrate all polarimeter functions in a single module which was robotically assembled. For this effort it is worth pursuing the integration of the amplifiers and mixers into a compact module.

There are several system constraints which must be factored in to the technology development effort. No single band can reasonably cover the full range of frequencies required to measure CO for $4 < z < 8$. Feedhorns and OMTs in this band will likely have waveguide interfaces so standardization on waveguide

bands is advantageous.

Goal 1: Ka-Band Receiver with less than 10 K noise. Given the state-of-the-art described above we can reasonably expect to develop a mass producible 26–40 GHz receiver front end with 8–10 K noise, gain of > 30 dB and IF bandwidth of 8 GHz. The receiver may require the use of 35 nm InP transistors or MMICs and will require either the development of a new mixer MMIC or cryogenic operation of existing commercial mixers. Design tradeoffs should also include the possible integration of signal modulation, which is especially important for the interferometer implementation.

Goal 2: K-Band Receiver with less than 10 K noise. An 18–26 GHz receiver does not currently exist. Again, the state-of-the-art suggests that 5–10 K noise is possible and should be pursued in an integrated mass-producible module. Design tradeoffs are likely to include device technology, MIC vs. MMIC integration, bare die vs. surface mount mixer technology as well as the system considerations outlined for the Ka-band receiver.

Goal 3: Ku-Band Receiver with 5 K noise. Again the state-of-the-art suggests this is a reasonable technology goal for the project. The receiver must cover the frequency range 12–18 GHz and design tradeoffs will be similar to Goal2.

6.2.5 ASIC-based cross-correlator designs

Power consumption by digital electronics is a significant issue for large arrays. We present here a summary of information from Dr Larry D'Addario, who has carried out a study of the effect of different correlator ASIC architectures on power consumption (Figure 6.9, (Navarro and D'Addario 2008; D'Addario 2008, 2011). This study was motivated by the worrisomely large operating cost of electricity for the SKA, but his results are relevant for any large-scale interferometer.

The input data buffer architecture (label as box [2] in Figure 6.9) is preferred. It uses slightly more power than architecture 1, but only 1/3 as many chips and much less I/O because it time-shares its CMACs among all baselines by using an input data buffer (Figure 6.10). For 2025 antennas and a bandwidth of 1 GHz (plausible SKA-mid dish array, which was the initial target of this ASIC architecture study), the power consumption of all chips is 25.8 kW. Adding 35% for power supplies. monitor and control chips, and other infrastructure gives a total power consumption of about 35 kW. This scales to about 88 kW for 1000 antennas and a bandwidth of 10 GHz.

For 50 antennas with 20 feeds each, and cross-correlating between antennas but not between feeds on the same antennas, we get a total correlator power consumption of only 4.3 kW for a bandwidth of 10 GHz. This design uses 640 ASICs.

D'Addario's ASIC architecture can be configured to work with a wide range of antenna numbers. In all cases each chip cross-correlates all baselines in the array, over a bandwidth that depends (inversely) on the number of antennas. For example, the same ASIC can be used for an array with 32 antennas or 2048 antennas—the trade is the number of chips needed per unit of observing bandwidth.

It should be noted that FPGA approaches require far more power than ASICs, and clusters of digital processing units or general-purpose CPUs are multiple orders of magnitude worse. CPU clusters also require very large numbers of boards, racks, and cooling compared with FPGA or ASIC designs. An

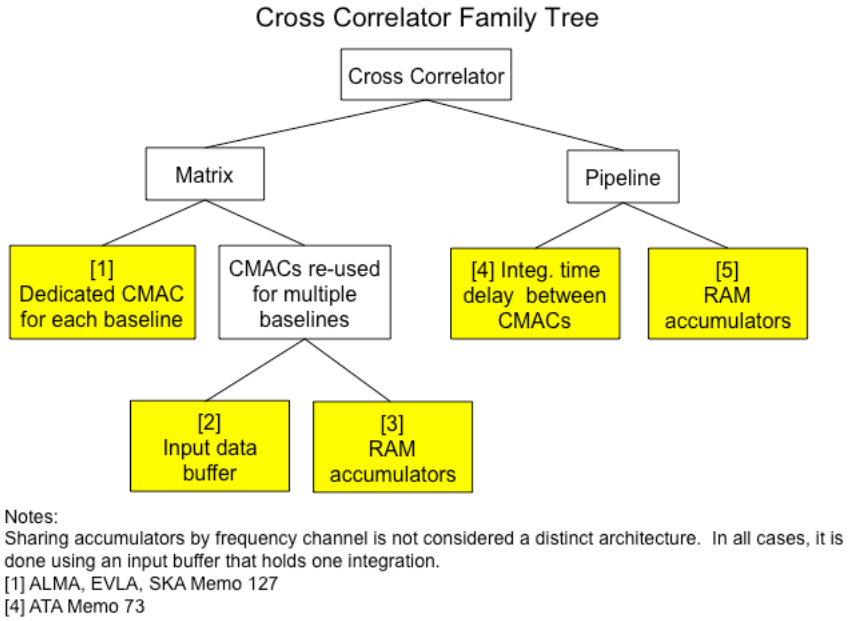

Figure 6.9: Overview of correlator architectures.

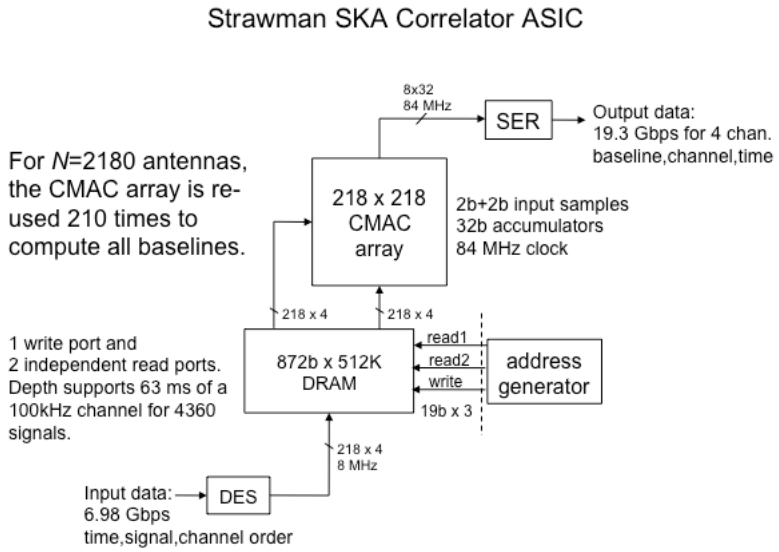

Figure 6.10: ASIC signal path on correlator architecture [2] in Figure 6.9.

Chip Type	Freq Channel Processing (F) Units	Correlation Processing (X) Units
ASIC *NEC CB-90*	180 chips 2 Racks	53 chips 1 Racks
FPGA *XC4VSX55*	360 chips 3 Racks	212 chips 2 Racks
DSP Processor *TMS320C6455*	4500 chips 30 Racks	19950 chips 125 Racks
General Purpose Processor *Intel T7700*	36000 chips 225 Racks	159600 chips 1000 Racks

Figure 6.11: Comparison of correlator architectures for an SKA-scale correlator.

early comparison for an SKA-scale correlator is in Figure 6.11. Based on this analysis, an ASIC-based correlator is likely justified for the ambitious high-z CO intensity mapping experiments.

6.2.6 Roadmap for CO line mapping

There are several areas where significant technical development is needed to enable the experiments described above. For the monopole experiment, measuring the integrated wide-field spectral fluctuations, a critical requirement is *extremely precise calibration of the instrumental bandpass response*. For this purpose extremely good absolute amplitude calibration is not essential, although a 1% error on the amplitude scale is desirable. Variations in the bandpass response will need to be calibrated to better than 1 part in 10^5. This implies a thermal aperture load whose emissivity over the observed frequency band is known, and whose internal temperature gradients are controlled or monitored, to this level.

For the CO-line mapping experiment, the technical challenges include *mass-producible low-cost integrated receiver modules* for 15 and 30 GHz and an *affordable concept for the large-scale digital signal processing* required. It should be noted that both of these areas are applicable to space missions as well. Low-mass feeds and other front end components are relevant for both planetary and Earth-sensing instruments, especially interferometers, and advances in scalable digital signal processing systems would benefit a wide range of future space missions and ground facilities (not least the SKA).

Given the large number of receiver modules (cooled feed, polarizer, and low noise amplifier, along with associated down-conversion if needed and digitizers) required at both 15 and 30 GHz, they need to be small, light, robust, and low-cost. Above, all they need to be designed for easy and reliable mass replication. This approach differs from the traditional design and fabrication techniques used for radio astronomy front ends.

The digital signal processing requirements for 1000-receiver systems with multi-gigahertz bandwidth, particularly for cross-correlation of signals, are challenging. Development of system-level architectures, detailed designs that minimize interconnections, memory use, and power consumption, and the selection of appropriate chip-level technologies are all areas where there is synergy with the SKA, an astronomy

project with even more challenging signal processing requirements. In this realm the challenge is not so much how to carry out the processing, but how to make it affordable.

In addition to these critical technology development areas, there are a number of somewhat more specific trade studies that are needed to prepare for a high-redshift CO mapping experiment. These include:

- Mechanical and cryogenic design of many feed (~ 1000) focal plane arrays for 15 and 30 GHz. This is challenging because of the large physical size of the array, especially at 15 GHz.
- Optimal geometric design for the telescopes in both cases.
- Consideration of fixed feed array vs. mounting on telescope (more feeds or less filling factor, but greater mechanical simplicity and stability).
- Observing site requirements (atmospheric emission, latitude, infrastructure, accessibility and operating costs).
- Direct digitization of RF band vs. downconversion before digitization.
- Digital vs. analog correlators.
- Operating flexibility needed to enable future science following CO line surveys.

In the longer term, observations of high-redshift lines at frequencies well above 30 GHz will need to be done from space. Early technology development for future 60 GHz and 200 GHz mapping missions are similar to those for the ground-based experiments—low mass front ends and low power digital processing. But the need to space-quality observing systems will inevitably mean that start-of-the-art components will have to be used, which will make the low power consumption goal more difficult to achieve.

6.3 Instrumentation for [C II] intensity mapping

For reionization-era experiments, [C II] is conveniently redshifted into the relatively-clear 1-mm atmospheric window which offers good transmission from 190 GHz to 310 GHz (corresponding to $z \sim 9$ to $z \sim 5$). The sensitivity is of course greater at the lower redshifts, and as Figure 5.8 shows, experiments at $z \sim 3.4$–3.8 and 4–4.6 may be tractable precursor measurements.

Table 6.2 presents our strawman [C II] instrument concept (see also Gong et al. 2012), with measurement parameters if coupled to 1, 3, and 10-meter apertures. The sensitivity to the mean intensity (or brightness temperature) is independent of aperture size, so 1 or 3-meter apertures can provide meaningful measurements early at modest cost and the few-arcminute angular scale would be a good match to a CO experiment on a $\sim$ 10-meter aperture, providing an opportunity for a cross-correlation. The larger apertures for [C II] provide access to the higher-k modes, which enable the cross-correlation with the 21 cm on the scalesize of the reionizing bubbles. CCAT, a leading facility for observations of discrete sources, could be considered, but the beamsize on CCAT at 250 GHz is ~ 15 arcsec. Thus relative to the smaller telesecopes, the same instrument using the full 25-meter CCAT aperture couples the higher-k modes at the expense of the lower-k modes, and is not particularly well-matched to measuring the clustering term, for example. Of course, in principle it would be possible to use a (few-meter) patch of the CCAT primary as the aperture, but the most cost-effective approach will likely be a small dedicated experiment.

Table 6.2:
EXPERIMENTAL PARAMETERS FOR A POSSIBLE CII MAPPING INSTRUMENT.

Aperture diameter (m)	1	3	10
Survey Area ($\deg^2$)	16	16	16
Total integration time (hours)	4000	4000	4000
Free spectral range (GHz)	185−310	185−310	185−310
Freq. resolution (GHz)	0.4	0.4	0.4
Number of bolometers	20,000	20,000	20,000
Number of spectral channels	312	312	312
Number of spatial pixels	64	64	64
Beam size[a] (FWHM, arcmin)	4.4	1.5	0.4
Beams per survey area[a]	2.6×10^3	2.3×10^4	2.6×10^5
$\sigma_{\rm pix}$: Noise per detector sensitivity[a] (Jy$\sqrt{\rm s}$/sr)	2.5×10^6	2.5×10^6	2.5×10^6
$T_{\rm pix}$: Integration time per beam[a] (hours)	100	11	1.0
$z = 6$ $V_{\rm pix}$ $({\rm Mpc/h})^3$	216.5	23.7	2.1
$z = 7$ $V_{\rm pix}$ $({\rm Mpc/h})^3$	332.4	36.8	3.3
$z = 8$ $V_{\rm pix}$ $({\rm Mpc/h})^3$	480.0	53.1	4.7
$z = 6$ $P_N^{\rm CII}$ $({\rm Jy/sr})^2$ $({\rm Mpc/h})^3$	3.7×10^9	3.7×10^9	3.6×10^9
$z = 7$ $P_N^{\rm CII}$ $({\rm Jy/sr})^2$ $({\rm Mpc/h})^3$	5.7×10^9	5.8×10^9	5.7×10^9
$z = 8$ $P_N^{\rm CII}$ $({\rm Jy/sr})^2$ $({\rm Mpc/h})^3$	8.3×10^9	8.4×10^9	8.1×10^9

[a] values computed at 238 GHz, corresponding to CII at $z = 7$.

The instrument approach is a background-limited wide-band dispersive spectrometer similar to Z-Spec (Bradford et al. 2010) but scaled up to ~ 100 spatial beams, and targeting a higher resolving power ($R = n/dn \sim 700$, corresponding to 5 comoving Mpc). Coherent systems such as SIS receivers as developed for ALMA might also be considered, but they are limited in bandwidth (e.g., 8 GHz which is dz of 0.34 at $z = 8$), and the enhanced spectral resolution offers no benefit except perhaps for very high-k modes. The broadband spectrometers can cover the full 190–310 GHz atmospheric window ($z = 6$–10) in a single observation. Furthermore, a direct-detection system can be made slightly more sensitive at a very good site. The strawman system uses 20,000 total bolometric detectors, arrayed spatially (~ 70 positions) and spectrally (~ 300 frequency bins).

The 20 kilo-pixel detector format is large but tractable for either the transitition-edge-sensed (TES) bolometers (e.g., Brevik et al. 2010) or the microwave kinetic-inductance detectors (MKID) (e.g., Maloney et al. 2010). Both of these technologies are being used by the Caltech/JPL superconducting detector group. Figure 6.12 shows the growth in far-IR/submm/mm detector format, and extrapolations into the future. 10–20 kilopixels is the break point at which the TES multiplexing becomes prohibitively expensive and realistically gives way to the simpler approach using microwave or RF multipexing with the MKID detectors. The required single-pixel detector sensitivities is 16×10^{-18} W Hz$^{-1/2}$, only a factor of three below that used on Z-Spec, and well within the demonstrated NEPs of TES bolometers in the laboratory.

While the detector array is tractable with existing technology, the spectrometer itself requires some development. Z-Spec was a scientific pathfinder for the [C II] intensity mapping experiment, but the waveguide grating approach is not well-suited to scaling up to 100 or more spectrometers. Members of this study are developing a new spectrometer approach using superconducting circuits patterned lithographically on silicon to create a spectrometer on a chip. The design is a bank of sequential $R \sim 700$ filters fed by a transmission line; each filter couples to an individual detector. The circuit model is outlined in a Caltech memo (Kovacs and Zmuidzinas 2011) and shown in Figure 6.13. Filterbanks have of course been used

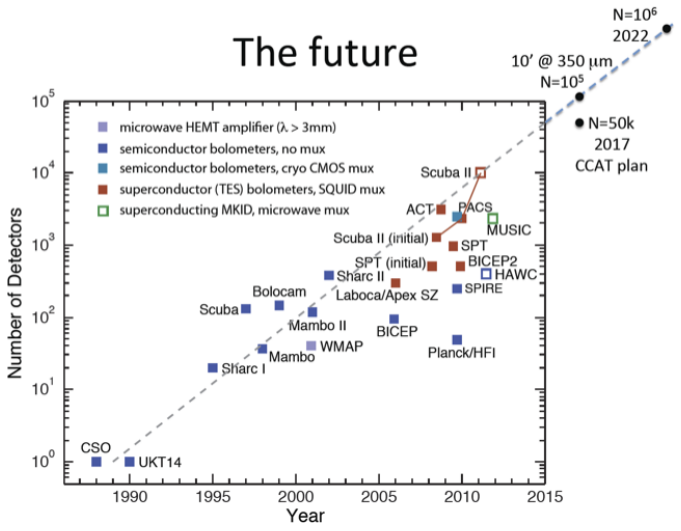

Figure 6.12: Growth in far-IR submillimeter detector format (credit: J. Zmuidzinas). The 10^4 pixel counts required for the [C II] mapping experiment are achievable now with either the SQUID-based or microwave multiplexer. Larger formats (10^5–10^6 pixels) for future experiments will likely be achieved with the microwave MUX which is simpler and more cost effective on large scales.

for decades in radio astronomy, and superconducting circuit technologies are now sufficiently mature that the entire system can be laid out in niobium transmission line. Figure 6.13 also shows some details of an approach under development to couple to the MKID detector. Coupling the incident radiation to the transmission line is readily accomplished with lithographed planar antennas, also in niobium. Such antenna systems are in use with the MUSIC camera and the SPIDER and BICEP2 CMB polarimeters, shown in Figure 6.14.

A simple demonstration of this new spectrometer technology would enable a modestly-priced first experiment with a 1–3 meter-class telescope at a high-altitude site (e.g., Mauna Kea or Chile). With the technologies in hand, a 10–20 kilopixel imaging spectrometer plus telescope capable of detecting the low-k autocorrelation in [C II] could be fielded for a few million dollars. We aim to undertake this spectrometer demonstration and the detailed instrument definition as part of a KISS follow-on study.

6.3.1 Roadmap for [C II] Line Mapping

EOR tomography in [C II] requires a high-throughput spectroscopic instrument to realize the sensitivity needed for [C II] fluctuation mapping. The Gong et al. (2012) study assumed 64 dispersive spectrometers operating 20,000 background-limited bolometers. The required detector noise equivalent power of NEP $\sim 3 \times 10^{-18}$ W Hz$^{-1/2}$ is well within achieved sensitivities for TES bolometers, and the detector count has been realized with the SCUBA2 instrument. MKID sensors are developing rapidly and may also be able to provide the required sensitivity. If so, use of MKIDs would greatly simplify the multiplexing system. The main challenge is therefore to develop compact focal plane spectrometer technology. Spectrometers fabricated in superconducting RF circuitry are very appealing, because the spectrometers are then integrated with the detectors in single planar lithographic fabrication, and the full spectrometer can be very compact. Similar spectrometer technologies are envisioned for CCAT for multi-object spectroscopy. A

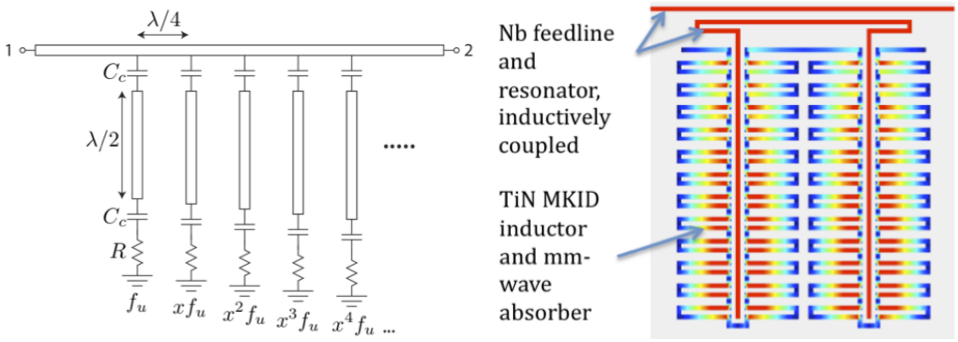

Figure 6.13: (*Left*) Concept for a superconducting filterbank spectrometer from (Kovacs and Zmuizinas 2011). Broadband radiation enters the transmission line at port 1 and propagates to the right. Each half-wave resonator acts as a filter to extract one spectral output channel. The channel spacing comparable to the filter width. The resistors R represent the dissipative loading of the detectors. (*Right*) Electromagnetic design of a feedline, resonator and detector. The feedline and resonator are niobium microstrip (1 μm wide on 1 μm silicon substrate) and show as red. The meandering structure is the titanium-nitride (TiN) inductor of an MKID; it is resistive at millimeter wavelengths, and absorbs the power from the resonator. Coupling between the feedline and resonator and between the resonator and the TiN are tuned by adjusting the spacing. As with all MKIDs, the power absorbed in the inductor results in an increased quasiparticle density, increasing the kinetic inductance and thus the resonant frequency of the microwave *LC* circuit.

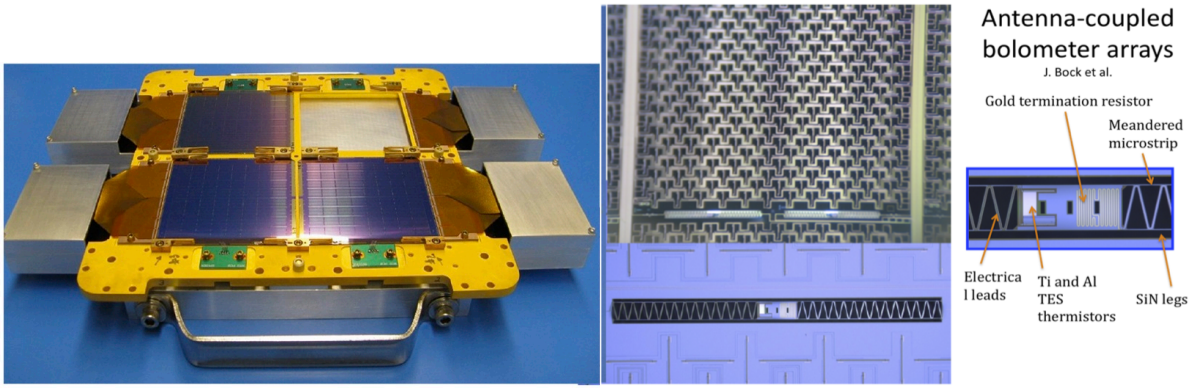

Figure 6.14: Antenna-coupled detector arrays used in the SPIDER CMB experiment, demonstrating planar antennas and large-scale lithographic circuitry. (Left) The full system consisting of 4 wafers tiled together. The total detector count is 512; 2 polarizations in 256 spatial pixels. (Right) A close up of one of the spatial pixels. Two separate (interleaved) antenna networks couple the two linear polarizations, each polarization then propagates on niobium microstrip to its detector island, a membrane of silicon-nitride. The microstrip is terminated in a gold resistor, raising the temperature of the island. The transition-edge (TES) superconducting thermistor is biased such that changes in photon power are exactly met by a reduction in the TES bias current (and thus power). The TES current is thus inversely proportional to the dissipated optical power.

backup system worth investigating would be a classical slit-fed grating spectrometer coupled to a sparsely filled 2-D focal-plane detector array. The rest of the instrument consists of a 4 K cryostat outfitted with a sub-K cooling system, similar to cooling systems already deployed in the Keck Polarimeter Array and Z-SPEC, and a 3-m class mm-wave telescope.

Because the instrument is modest in scope, we intend to focus effort on demonstrating the enabling 2-D on chip spectrometer technology. This is largely an optical demonstration, and will be pursued independent of the final detector technology. With a demonstration of the spectrometer in hand, we would be in good position to propose the full instrument to NSF. The full roadmap includes the following technology development and design studies:

- Lithographed spectrometer materials assessment. We will first determine propagation loss for dielectrics. Improvements are required relative to the existing measurements with Nb/SiO_2/Nb, and we will measure silicon nitride, and amorphous and crystal silicon. Test devices for investigating loss have already been in designed so this development can proceed quickly.

- Spectrometer design. Resonant or "filter-bank" spectrometers are the most appealing choice because they are path-folding devices and thus very compact. These systems can be realized in microstrip or CPW depending on propagation loss. Another option is a planar grating design in microstrip. The final choice depends on the propagation loss, required fabrication tolerances, and channel-to-channel cross talk.

- Spectrometer demonstration. Develop a test spectrometer with a few tens of channels to demonstrate optical efficiency, band definition, and cross-talk.

In addition, we need to investigate the following system-level issues

- Design of the focal plane. The spectrometers can be coupled to planar antennas, which allows for planar lithographic fabrication. The detectors however can couple to stray radiation. For TES polarimeters, the measured stray coupling is $\sim$0.5% in power for a 25% spectral band, which could become serious for a spectrometer with 100 times higher resolving power (100 $\times$ smaller spectral band per detector). Either the detectors can be located away from the antenna and shielded by a layer of Nb groundplane, or we can use feedhorn coupling and enclose the spectrometer. We will also investigate the slit-fed grating spectrometer design as a backup.

- The instrument site must be decided, considering susceptibility to atmospheric noise and 21 cm survey partnership.

- A detailed system design, including an assessment of astrophysical systematics, such as Galactic continuum susceptibility, will strengthen the case for NSF funding. This study can also explore the case for a few high-frequency channels to map [C II] emission at lower redshifts.

6.4 Lyman-α Line Mapping

The scientific case for Ly-α tomographic mapping currently lags behind the published theoretical studies for CO and [C II] mapping experiments. However Ly-α line mapping is an excellent fit to a SMEX space opportunity, since it requires a small telescope aperture, existing infrared detector arrays operating out to

2.5 μm, and a simple passive cooling system. Furthermore it may be possible to carry out narrow-band imaging from the ground as a scientific demonstration at 0.8–2.0 μm from the ground in limited clean spectral bands between the narrow but bright airglow lines. The scientific case for Ly-α mapping will rapidly evolve, with theoretical papers in preparation and results from the CIBER instrument expected to both emerge in the next six months. Limited theoretical effort is appropriate at this early stage, but the results should be carefully monitored for an emerging and timely experimental opportunity.

7

Conclusions

The First Billion Years Study Program sought to identify unique opportunities to probe the formation and evolution of structure in the early Universe and the large-scale consequences of the interaction of baryons and Dark Matter. The Study Program successfully identified two new observational avenues to accomplish this objective with the potential to yield fundamental discoveries in basic physics and cosmology. Both approaches exploit spectral line deviations imprinted on the CMB blackbody spectrum to

1. better constrain inflation, time-variation of fundamental physical constants, and pre-recombination radiation processes, including dark matter annihilation and decay, by targeting H and He recombination lines that should appear today as tiny deviations from the all-sky (monopole) blackbody spectrum of the CMB, and

2. provide the only foreseeable maps in CO and [C II] of large-scale structure during the epoch of reionization that can be cross-correlated with upcoming redshifted 21 cm maps to provide a definitive, model-independent test of the inside-out hypothesis of reionization evolution.

Both ground-based and space-based platforms will be needed to fully study the cosmological signals, and technical developments will be needed in several areas. The Study concluded that technical work is most urgent for the CO and [C II] intensity mapping programs, and we present roadmaps for these. The technical development for CO mapping will also be useful for the even more difficult recombination line studies.

The all-sky monopole observations and the CO intensity mapping observations share a core set of common instrumental requirements based on the need to deploy 100 to 1000 feed elements each and derive broadband spectra with resolutions of order $R = 1000$. A roadmap of technical development that leads to instruments that meet the requirements of the desired observations was developed that articulates a unified, staged path for the technical research and development and exploits the ground-based CO intensity mapping instrument as a technology testbed and precursor for the more complicated and more long-term space-based recombination line experiment. In parallel, the participants laid out a roadmap of technical developments needed to enable a high-throughput spectroscopic instrument for [C II] fluctuation mapping.

The participants in the Study Program plan to use these roadmaps to pursue funding opportunities for instrument development.

The Study Program initiated theoretical inquiry into a variety of outstanding questions regarding the nature of the recombination line and large-scale CO signals and the properties of spinning dust and other foregrounds that will have both immediate and long-term benefits for other areas of astrophysics. New ideas for observations with existing facilities were developed during the Program.

7.1 Expected papers

Three independent theoretical papers addressing CO signal strength calculations and cross-correlation predictions for CO and 21 cm maps were initiated during the Study Program. The three lead authors are Carilli, Cooray, and Furlanetto. The papers treat both analytic estimates and numerical simulations of large-scale structure as traced by CO line emission between redshifts 6 and 10.

Two theoretical papers are planned to better develop the science case for recombination line spectral distortion observations. The first is a calculation of the effect of time variation of the fundamental constant, α, on the recombination spectrum; the second a calculation of the decaying dark matter contribution to the recombination spectrum. Both papers will be led by Chluba.

Theoretical modeling of individual molecular line contributions to the spinning dust anomalous emission model is planned and a paper is anticipated to result from this work. The primary author will be Ali-Haïmoud.

The Study participants identified the goal of working toward a detailed instrument design whitepaper for the CO intensity mapping experiment. Additional funding will be sought to complete this effort.

Precursor observations on EVLA, MeerKat, ALMA, and smaller institutional instruments will be pursued to better constrain the foreground properties and CO signal strength estimates. Upon completion, results of these observations will be published.

7.2 Proposal opportunities

Several technology development proposal opportunities have been identified:

- Low-mass feed design, fabrication, and performance
- Integrated receiver module design, fabrication, and performance
- Cryogenic systems for 1000-element focal plane arrays
- Direct digitization vs. downconversion (trade study)
- Large-scale correlator architecture (with power and cost estimates)
- Application of ultra-low-power IC technologies to signal processing
- 2D spectrometer technology for [C II] mapping

Ground-based experiment proposal opportunities:

- Deep spectral observation of bright high-latitude radio source to determine level of spectral flatness obtainable, limits of scattered line contamination)
- Pathfinder recombination line experiment
- A CO dual-frequency mapping experiment (both hemispheres)
- A [C II] mapping experiment

Space-based mission proposal opportunities:

- Monopole recombination line experiment
- 60 and/or 200 GHz mapping experiment(s)

7.3 Acknowledgements

This Study was supported by the Keck Institute of Space Studies and the JPL Office of the Chief Scientist and Chief Technologist. We thank Michele Judd, Exie Marie Leagons, and Paula Lonergan for their contributions coordinating the August and November workshops, and for generously going above and beyond the call of duty to make the Study not only a productive scientific endeavor, but also a fun experience and rare opportunity to building last relationships with our colleagues on a personal level. Thank you!

References

Abraham, P., C. Leinert, and D. Lemke (1997, December). Search for brightness fluctuations in the zodiacal light at 25 MU M with ISO. *A&A 328*, 702–705.

Barkana, R. and A. Loeb (2005, May). A Method for Separating the Physics from the Astrophysics of High-Redshift 21 Centimeter Fluctuations. *ApJL 624*, L65–L68.

Bock, J., J. Battle, A. Cooray, M. Kawada, B. Keating, A. Lange, D.-H. Lee, T. Matsumoto, S. Matsuura, S. Pak, T. Renbarger, I. Sullivan, K. Tsumura, T. Wada, and T. Watabe (2006, March). The cosmic infrared background experiment. *New Astronomy Reviews 50*, 215–220.

Bradford, C. M., J. Bock, W. Holmes, M. Kenyon, A. Beyer, M. Werner, M. Rud, T. Prouvé, P. Echternach, K. Irwin, S. Cho, M. Harwit, G. Stacey, G. Helou, L. Armus, P. Appleton, J. D. Smith, U. Gorti, G. Rieke, E. Egami, D. Lester, J. Glenn, M. Malkan, and D. Dale (2010, July). The background-limited infrared-submillimeter spectrograph (BLISS) for SPICA: a design study. In *Society of Photo-Optical Instrumentation Engineers (SPIE) Conference Series*, Volume 7731 of *Society of Photo-Optical Instrumentation Engineers (SPIE) Conference Series*.

Brevik, J. A., R. W. Aikin, M. Amiri, S. J. Benton, J. J. Bock, J. A. Bonetti, B. Burger, C. D. Dowell, L. Duband, J. P. Filippini, S. R. Golwala, M. Halpern, M. Hasselfield, G. Hilton, V. V. Hristov, K. Irwin, J. P. Kaufman, B. G. Keating, J. M. Kovac, C. L. Kuo, A. E. Lange, E. M. Leitch, C. B. Netterfield, H. T. Nguyen, R. W. Ogburn, IV, A. Orlando, C. Pryke, C. Reintsema, S. Richter, J. E. Ruhl, M. Runyan, C. Sheehy, Z. Staniszewski, R. Sudiwala, J. E. Tolan, A. D. Turner, P. Wilson, and C. L. Wong (2010, July). Initial performance of the BICEP2 antenna-coupled superconducting bolometers at the South Pole. In *Society of Photo-Optical Instrumentation Engineers (SPIE) Conference Series*, Volume 7741 of *Society of Photo-Optical Instrumentation Engineers (SPIE) Conference Series*.

Bunton, J. (2007). Dish cost frequency scaling. Memo 90, Square Kilometer Array.

Cantalupo, S., C. Porciani, and S. J. Lilly (2008, January). Mapping Neutral Hydrogen during Reionization with the Lyα Emission from Quasar Ionization Fronts. *ApJ 672*, 48–58.

Carilli, C. L. (2011, April). Intensity Mapping of Molecular Gas During Cosmic Reionization. *ApJL 730*, L30.

Chang, T.-C., U.-L. Pen, K. Bandura, and J. B. Peterson (2010, July). An intensity map of hydrogen 21-cm emission at redshift z˜0.8. *Nature 466*, 463–465.

Chluba, J. (2010, February). Could the cosmological recombination spectrum help us understand annihilating dark matter? *MNRAS 402*, 1195–1207.

Chluba, J. and R. A. Sunyaev (2006, November). Free-bound emission from cosmological hydrogen recombination. *A&A 458*, L29–L32.

Chluba, J. and R. A. Sunyaev (2008a, September). Evolution of low-frequency features in the CMB spectrum due to stimulated Compton scattering and Doppler broadening. *A&A 488*, 861–865.

Chluba, J. and R. A. Sunyaev (2008b, February). Is there a need and another way to measure the cosmic microwave background temperature more accurately? *A&A 478*, L27–L30.

Chluba, J. and R. A. Sunyaev (2008c, March). Two-photon transitions in hydrogen and cosmological recombination. *A&A 480*, 629–645.

Chluba, J. and R. A. Sunyaev (2009, July). Pre-recombinational energy release and narrow features in the CMB spectrum. *A&A 501*, 29–47.

Chluba, J. and R. A. Sunyaev (2010, February). Cosmological recombination: feedback of helium photons and its effect on the recombination spectrum. *MNRAS 402*, 1221–1248.

Chluba, J., G. M. Vasil, and L. J. Dursi (2010, September). Recombinations to the Rydberg states of hydrogen and their effect during the cosmological recombination epoch. *MNRAS 407*, 599–612.

Cooray, A., J. J. Bock, B. Keatin, A. E. Lange, and T. Matsumoto (2004, May). First Star Signature in Infrared Background Anisotropies. *ApJ 606*, 611–624.

D'Addario, L. R. (2008). Antenna cost modeling for large arrays. In *URSI National Radio Science Meeting, Boulder*, Volume Paper J4-1.

D'Addario, L. R. (2011). Low power correlator architectures for large radio astronomy correlators. Memo 133, Square Kilometer Array.

De Lucia, G. and J. Blaizot (2007, February). The hierarchical formation of the brightest cluster galaxies. *MNRAS 375*, 2–14.

DeBoer, D. (2006). Technical report, Square Kilometer Array Meeting, Paris.

Dubrovich, V. K. (1975, October). Hydrogen recombination lines of cosmological origin. *Soviet Astronomy Letters 1*, 196.

Furlanetto, S. R., S. P. Oh, and F. H. Briggs (2006, October). Cosmology at low frequencies: The 21 cm transition and the high-redshift Universe. *Physics Reports 433*, 181–301.

Furlanetto, S. R., J. Schaye, V. Springel, and L. Hernquist (2003, December). Mapping the Cosmic Web with Lyα Emission. *ApJL 599*, L1–L4.

Gong, Y., A. Cooray, M. Silva, M. G. Santos, J. Bock, C. M. Bradford, and M. Zemcov (2012, January). Intensity Mapping of the [C II] Fine Structure Line during the Epoch of Reionization. *ApJ 745*, 49.

Gong, Y., A. Cooray, M. B. Silva, M. G. Santos, and P. Lubin (2011, February). Probing Reionization with Intensity Mapping of Molecular and Fine-structure Lines. *ApJL 728*, L46.

Illarionov, A. F. and R. A. Siuniaev (1975, June). Comptonization, the background-radiation spectrum, and the thermal history of the universe. *Soviet Astronomy 18*, 691–699.

Kashlinsky, A., R. G. Arendt, J. Mather, and S. H. Moseley (2005, November). Tracing the first stars with fluctuations of the cosmic infrared background. *Nature 438*, 45–50.

Kovacs, A. and J. Zmuizinas (2011). Transmission-line resonator spectrometers. Internal memorandum, California Institute of Technology.

Kutyrev, A. S., R. Arendt, E. Dwek, S. H. Moseley, D. Rapchun, and R. F. Silverberg (2008, August). High efficiency near infrared spectrometer for zodiacal light spectral study. In *Society of Photo-Optical Instrumentation Engineers (SPIE) Conference Series*, Volume 7014 of *Society of Photo-Optical Instrumentation Engineers (SPIE) Conference Series*.

Lidz, A., S. R. Furlanetto, S. P. Oh, J. Aguirre, T.-C. Chang, O. Doré, and J. R. Pritchard (2011, November). Intensity Mapping with Carbon Monoxide Emission Lines and the Redshifted 21 cm Line. *ApJ 741*, 70.

Lidz, A., O. Zahn, S. R. Furlanetto, M. McQuinn, L. Hernquist, and M. Zaldarriaga (2009, January). Probing Reionization with the 21 cm Galaxy Cross-Power Spectrum. *ApJ 690*, 252–266.

Lyubarsky, Y. E. and R. A. Sunyaev (1983, July). The spectral features in the microwave background spectrum due to energy release in the early universe. *A&A 123*, 171–183.

Madden, S. C., M. Galametz, D. Cormier, V. Lebouteiller, F. Galliano, S. Hony, A. Rémy, M. Sauvage, A. Contursi, E. Sturm, A. Poglitsch, M. Pohlen, M. W. L. Smith, G. Bendo, and B. O'Halloran (2011, November). The Elusive ISM of Dwarf Galaxies: Excess Submillimetre Emission & CO-Dark Molecular Gas. In M. Röllig, R. Simon, V. Ossenkopf, & J. Stutzki (Ed.), *EAS Publications Series*, Volume 52 of *EAS Publications Series*, pp. 95–101.

Maloney, P. R., N. G. Czakon, P. K. Day, T. P. Downes, R. Duan, J. Gao, J. Glenn, S. R. Golwala, M. I. Hollister, H. G. Leduc, B. A. Mazin, S. G. McHugh, O. Noroozian, H. T. Nguyen, J. Sayers, J. A. Schlaerth, S. Siegel, J. E. Vaillancourt, A. Vayonakis, P. Wilson, and J. Zmuidzinas (2010, July). MUSIC for sub/millimeter astrophysics. In *Society of Photo-Optical Instrumentation Engineers (SPIE) Conference Series*, Volume 7741 of *Society of Photo-Optical Instrumentation Engineers (SPIE) Conference Series*.

Martin, C., A. Moore, P. Morrissey, M. Matuszewski, S. Rahman, S. Adkins, and H. Epps (2010). The keck cosmic web imager. In I. S. McLean, S. K. Ramsay, and H. Takami (Eds.), *Society of Photo-Optical Instrumentation Engineers (SPIE) Conference Series*, Volume 7735, pp. 77350M.

Matsumoto, T., H. J. Seo, W.-S. Jeong, H. M. Lee, S. Matsuura, H. Matsuhara, S. Oyabu, J. Pyo, and T. Wada (2011, December). AKARI Observation of the Fluctuation of the Near-infrared Background. *ApJ 742*, 124.

Matuszewski, M., D. Chang, R. M. Crabill, D. C. Martin, A. M. Moore, P. Morrissey, and S. Rahman (2010, July). The Cosmic Web Imager: an integral field spectrograph for the Hale Telescope at Palomar Observatory: instrument design and first results. In *Society of Photo-Optical Instrumentation Engineers (SPIE) Conference Series*, Volume 7735 of *Society of Photo-Optical Instrumentation Engineers (SPIE) Conference Series*.

Morales, M. F. and J. S. B. Wyithe (2010, September). Reionization and Cosmology with 21-cm Fluctuations. *A. Rev. Astr. Astrophys. 48*, 127–171.

Navarro, R. and L. R. D'Addario (2008). Scaling correlator architecture to large arrays of antennas. In *URSI National Radio Science Meeting, Boulder*.

Ono, Y., M. Ouchi, B. Mobasher, M. Dickinson, K. Penner, K. Shimasaku, B. J. Weiner, J. S. Kartaltepe, K. Nakajima, H. Nayyeri, D. Stern, N. Kashikawa, and H. Spinrad (2012, January). Spectroscopic Confirmation of Three z-dropout Galaxies at z = 6.844-7.213: Demographics of Lyα Emission in z ˜ 7 Galaxies. *ApJ 744*, 83.

Ouchi, M., K. Shimasaku, H. Furusawa, T. Saito, M. Yoshida, M. Akiyama, Y. Ono, T. Yamada, K. Ota, N. Kashikawa, M. Iye, T. Kodama, S. Okamura, C. Simpson, and M. Yoshida (2010, November). Statistics of 207 Lyα Emitters at a Redshift Near 7: Constraints on Reionization and Galaxy Formation Models. *ApJ 723*, 869–894.

Peebles, P. J. E. (1968, July). Recombination of the Primeval Plasma. *ApJ 153*, 1.

Pirzkal, N., S. Malhotra, J. E. Rhoads, and C. Xu (2007, September). Optical-to-Mid-Infrared Observations of Lyα Galaxies at z˜5 in the Hubble Ultra Deep Field: A Young and Low-Mass Population. *ApJ 667*, 49–59.

Pritchard, J. R. and A. Loeb (2011, September). 21-cm cosmology. *ArXiv e-prints*, arXiv:1109.6012.

Rubiño-Martín, J. A., J. Chluba, and R. A. Sunyaev (2006, October). Lines in the cosmic microwave background spectrum from the epoch of cosmological hydrogen recombination. *MNRAS 371*, 1939–1952.

Rubiño-Martín, J. A., J. Chluba, and R. A. Sunyaev (2008, July). Lines in the cosmic microwave background spectrum from the epoch of cosmological helium recombination. *A&A 485*, 377–393.

Schenker, M. A., D. P. Stark, R. S. Ellis, B. E. Robertson, J. S. Dunlop, R. J. McLure, J.-P. Kneib, and J. Richard (2012, January). Keck Spectroscopy of Faint $3 < z < 8$ Lyman Break Galaxies: Evidence for a Declining Fraction of Emission Line Sources in the Redshift Range $6 < z < 8$. *ApJ 744*, 179.

Stacey, G. J., S. Hailey-Dunsheath, C. Ferkinhoff, T. Nikola, S. C. Parshley, D. J. Benford, J. G. Staguhn, and N. Fiolet (2010, December). A 158 μm [C II] Line Survey of Galaxies at z ˜ 1-2: An Indicator of Star Formation in the Early Universe. *ApJ 724*, 957–974.

Stark, D. P., R. S. Ellis, K. Chiu, M. Ouchi, and A. Bunker (2010, November). Keck spectroscopy of faint $3 < z < 7$ Lyman break galaxies - I. New constraints on cosmic reionization from the luminosity and redshift-dependent fraction of Lyman α emission. *MNRAS 408*, 1628–1648.

Stark, D. P., R. S. Ellis, J. Richard, J.-P. Kneib, G. P. Smith, and M. R. Santos (2007, July). A Keck Survey for Gravitationally Lensed Lyα Emitters in the Redshift Range $8.5<z<10.4$: New Constraints on the Contribution of

Low-Luminosity Sources to Cosmic Reionization. *ApJ 663*, 10–28.

Sunyaev, R. A. and J. Chluba (2009, July). Signals from the epoch of cosmological recombination (Karl Schwarzschild Award Lecture 2008). *Astronomische Nachrichten 330*, 657.

Tielens, A. G. G. M. and D. Hollenbach (1985, April). Photodissociation regions. I - Basic model. II - A model for the Orion photodissociation region. *ApJ 291*, 722–754.

Visbal, E. and A. Loeb (2011, May). Measuring the 3D Clustering of Undetected Galaxies Through Cross Correlation of their Cumulative Flux Fluctuations from Multiple Spectral Lines. In *American Astronomical Society Meeting Abstracts #218*, pp. 120.04.

Visbal, E., H. Trac, and A. Loeb (2011, August). Demonstrating the feasibility of line intensity mapping using mock data of galaxy clustering from simulations. *J. Cosmology Astroparticle Phys. 8*, 10.

Wang, R., J. Wagg, C. L. Carilli, F. Walter, D. A. Riechers, C. Willott, F. Bertoldi, A. Omont, A. Beelen, P. Cox, M. A. Strauss, J. Bergeron, T. Forveille, K. M. Menten, and X. Fan (2011, September). CO (2-1) Line Emission in Redshift 6 Quasar Host Galaxies. *ApJL 739*, L34.

Weinreb, S. (2006). Ska antenna and receiver cost optimization including survey speed and focalplane arrays. Memo 77, Square Kilometer Array.

Zeldovich, Y. B., V. G. Kurt, and R. A. Syunyaev (1968, July). Recombination of Hydrogen in the Hot Model of the Universe. *Zhurnal Eksperimental noi i Teoreticheskoi Fiziki 55*, 278–286.